STANDARDIZATION OF A CAPACITIVE BRIDGE DEVICE FOR BULK "ENGINEERING" MAGNETOSTRICTION MEASUREMENTS IN FERROMAGNETIC MATERIALS

An Abstract of a Thesis
Presented to the
Faculty of the Physics Department
Western Illinois University

In Partial Fulfillment
of the Requirements for the Degree
Master of Science

by
Naveen Kumar Jha
May 2002

ABSTRACT

Magnetostriction effects have been investigated for five different materials by using a simple, reproducible, and cost-effective method just recently developed (last year) in our research laboratory. The current study has served to standardize the measurement device and verify its calibration with well-known standard materials of high purity. The magnetostriction effects in our samples were generated by a large oscillating magnetic field produced by a high current 60 Hz AC power supply, and then detected via a change in capacitance between a hollow cylindrical sample and a concentric brass ring, monitored at a high frequency rate by an older-model analog standard laboratory capacitance bridge meter whose null output was connected to a storage CRO and computer for follow-up analysis. Four ferromagnetic rings, constructed of highly purified nickel and iron for purposes of standard textbook comparison, and of high-speed steels 4620 and 4340 (which have proven applicability for use in magneto-elastic torque sensing), were used as the samples for investigating the magnetostriction effects, while a paramagnetic aluminum ring was used for the control sample to verify the zeroing and paramagnetic correction factors for our apparatus. The values of the engineering magnetostriction coefficients in ppm thus determined have been found to be in excellent agreement with standard tabulated values in the literature for nickel and iron, and with more recently published experimental values and torque sensor applicabilities for the two steel alloys. We have found this new measurement method to be both reproducible and reliable in determining “engineering” values of the magnetostriction constants for ferromagnetic materials.

ACKNOWLEDGEMENTS

I would like to acknowledge my thesis advisor Dr. Mark S. Boley. Without his efforts and encouragements, this work would not ever have come into this form. I sincerely thank him for his tremendous enthusiasm in making me continue to work and providing his proper guidance. I appreciate his full devotion and all of his valuable time he spent on this thesis. Without his efforts and constant pressure I could not have finished on time.

I would also like to thank Dr. H. B. Hart and especially Professor Doug Franklin for his helpful suggestions and corrections during the writing of this thesis. I would also like to thank Jennifer Rabchuk and Dr. Jim Rabchuk for providing me with an opportunity to study the Bible, and also for Dr. Rabchuk and Dr. Boley who prayed for me during my stay here at WIU.

My acknowledgements would be incomplete without thanking my awesome friends, No Soung Myoung, Laurie Pichla, Matthew Tillman, Michael Baxa, Jason Wilson, Ryan Wright, Jason T. Orris, J. C. Gumbart, and Christine Battaglia. I would also like to thank Yew Li Hor, Anup Pandey, and Manea Alkhalifah for their moral support during this semester, when I needed it the most. I appreciate Tin Tin Khine and Sunil Shrestha for their help during my stay here at WIU.

Finally, I deeply appreciate Manesh Pradhan and Pranay and his family for their wonderful words of support and for providing me with an opportunity to stay with them last summer.

STANDARDIZATION OF A CAPACITIVE BRIDGE DEVICE FOR BULK "ENGINEERING" MAGNETOSTRICTION MEASUREMENTS IN FERROMAGNETIC MATERIALS

A Thesis
Presented to the
Faculty of the Physics Department
Western Illinois University

In Partial Fulfillment
of the Requirements for the Degree
Master of Science

by
Naveen Kumar Jha
May 2002

TABLE OF CONTENTS

LIST OF FIGURES

Figure **Page**

Chapter 1: Introduction

Chapter 2: Theory

Chapter 3: Experimental setup

Chapter 4: Data collection and Analysis

LIST OF TABLES

Table **Page**

Chapter 1. Introduction

1-1. Magnetostriction

Ferromagnetic materials possess a tendency to change their crystalline dimensions when placed in a strong magnetic field. Materials such as iron, cobalt, nickel, and their alloys demonstrate this effect of expansion or contraction due to an externally applied changing magnetic field, and this is known as magnetostriction. This effect also implies that a change in magnetic field occurs when dimensions are forcefully changed. If a piece of ferromagnetic material is placed in a weak magnetic field, some of the favorably oriented domains grow slightly and smoothly at the expense of others. As the intensity of the magnetic field is further increased these domains continue to grow by steps, eventually taking over the less favorably oriented domains. This process continues until each crystal becomes one large domain. The reason is that the crystalline lattice inside each domain is spontaneously deformed in the direction of domain magnetization and its strain axis rotates with a rotation of the domain magnetization, thus resulting in a deformation of the specimen as a whole as shown in Figure 1-1. The specimen then is magnetized in the direction of least opposition, the direction which most nearly coincides with that of the external magnetic field. During this process the material expands (or contracts), along some or all of its dimensions. When all the domains are parallel to the field, the material is said to be saturated, as shown in Figure 1-2. The change in dimension ($\Delta l/l$) due to magnetostriction is on the order of 10^{-6} of the original dimension and is usually measured in parts per million (ppm). The measurement of such small changes in dimension can be a tremendous challenge.

Figure 1-1. Rotation of domain magnetization and accompanying rotation of the axis of spontaneous strain.

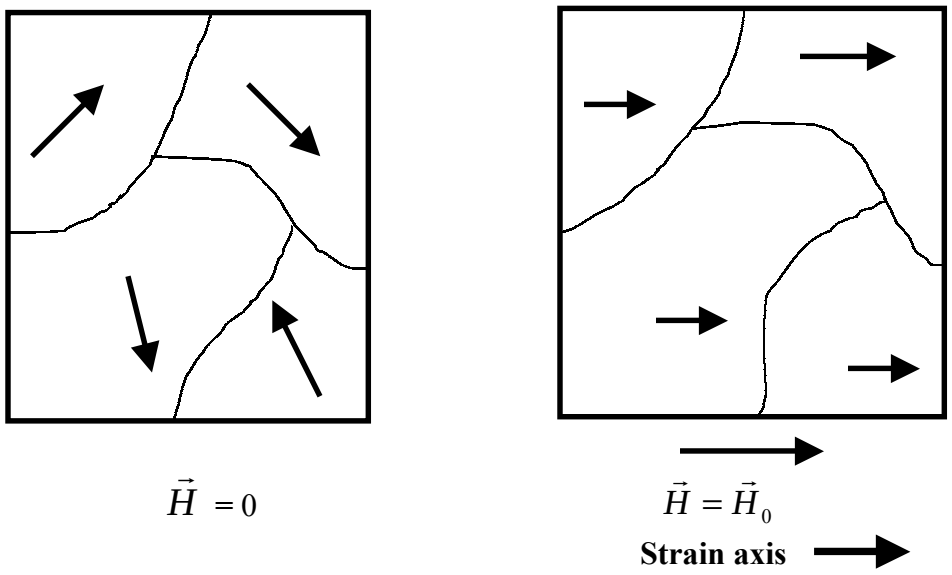

Figure 1-2. Magnetostriction as a function of the field intensity.

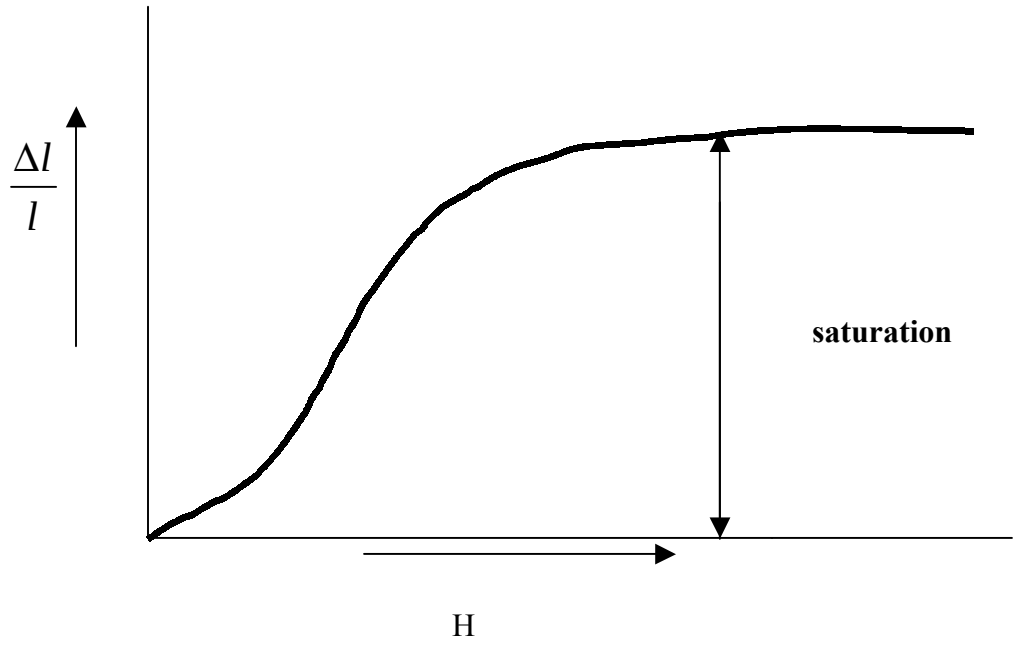

1-2. Measurement of Magnetostriction

Until recently magnetostriction was largely of theoretical interest and had only limited technological importance. The theoretical importance of magnetostriction was emphasized early on primarily by McKeehan, Akulov, Becker, and his colleagues[1]. Magnetostrictive elements can be used in oscillatory circuits to control frequencies from 1000 to 100,000 cycles per second. However, a present-day technological application recently receiving wide attention is their use as torque sensors in automotive power steering systems and in automotive transmission systems.

The challenge of measuring the magnetostriction effects was originally met by use of a strain gauge technique[2]. Another older method of measurement used mechanical and optical levers[3] but it was not routinely performed in the laboratory because of its complexity. An easier method of determining the magnetostriction constant is to use a single crystal disk, the two sides of which are cut parallel, to measure the increase in length during the revolution of magnetization in the plane of the disk. The convenient procedure for doing this is to attach two strain gauges, one parallel to the [001] plane on the top surface and the other parallel to the gap of an electromagnet, and then rotate the direction of magnetization in the crystal by rotating the electromagnet or by rotating the specimen itself[4].

Similarly, older methods of measuring magnetostriction are shown in Figure 1-3 and in Figure 1-4. The specimen is attached to a strip, as shown in Figure 1-3, and the change in length of the specimen is measured by attaching a thread that rests on and turns a carefully constructed roller on which there is a mirror attached. The rotation of the mirror is observed by a telescope or by light and scale. Similarly as shown in Figure 1-4,

Figure 1-3. Measurement of magnetostriction, where the change in length of the specimen moves a lever arm to which is attached a wire that turns a mirror, which then moves a reflected light beam on the scale. Figure reprinted from Bozorth (1920).

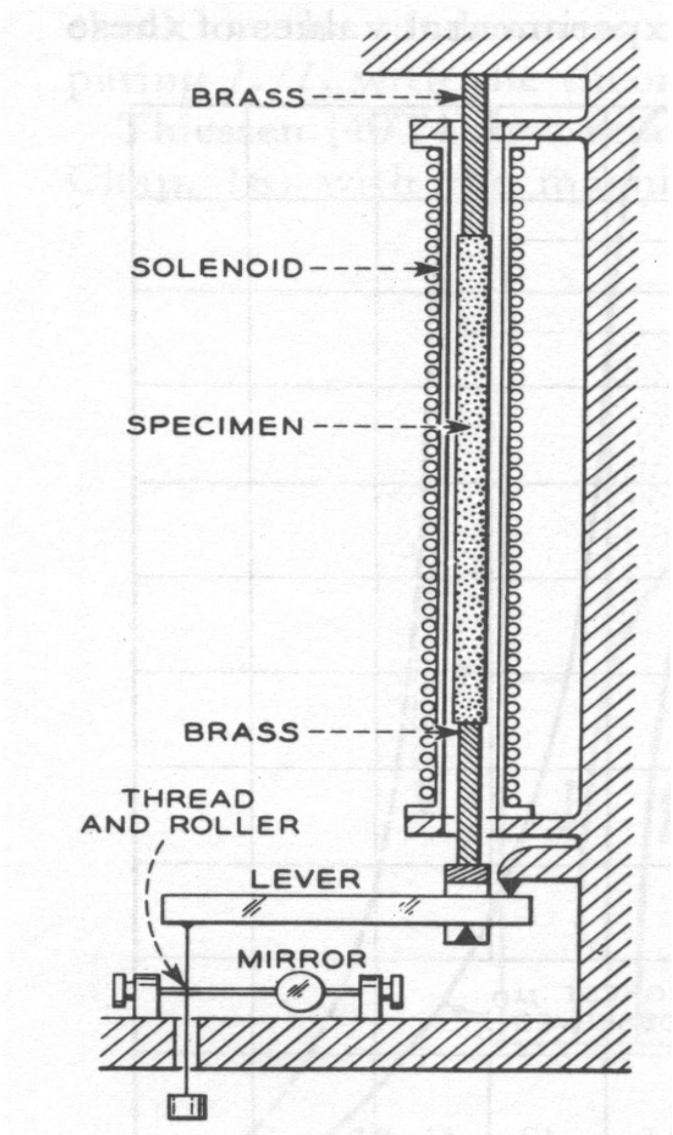

Figure 1-4. Determination of volume magnetostriction by movement of the meniscus of a liquid. Figure reprinted from Bozorth (1900).

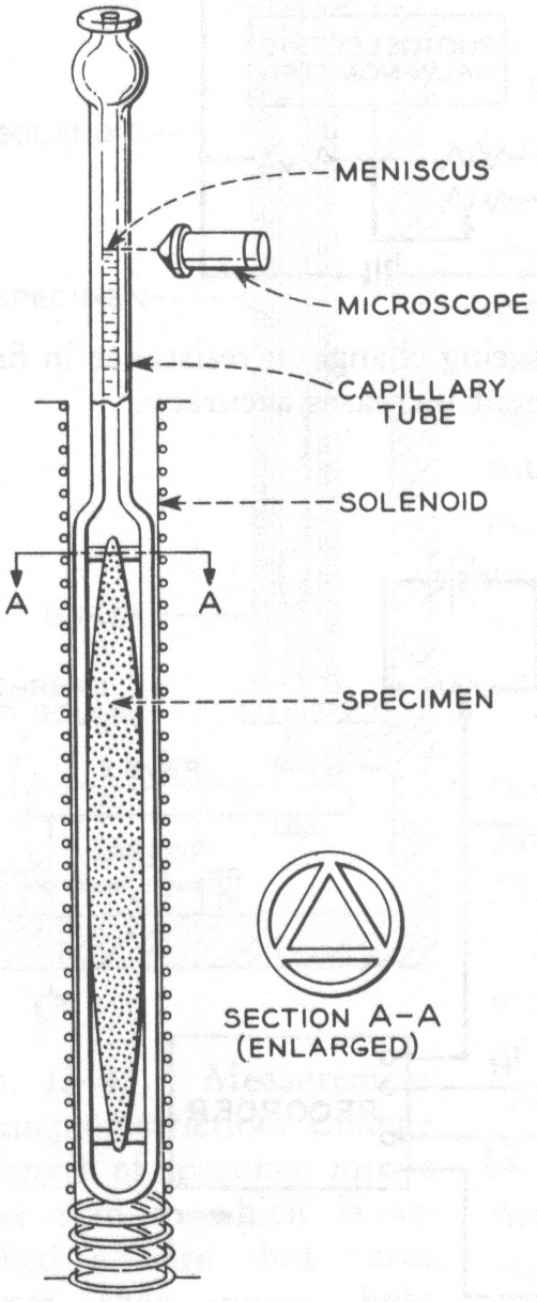

yet another method of measurement of magnetostriction by Nagaoka and Honda[5] in 1900 is a measurement of the actual change of volume due to magnetostriction effects. The specimen is kept inside a liquid with a glass capillary sealed to the top of the vessel. O'Conner and Fawcett[6] first introduced the method of using a parallel plate capacitor to measure magnetostriction. In this simple case, a sample is attached to the plates, and a change of its length causes the change in distance between the plates. By measuring the change in capacitance it is therefore possible to calculate the change in dimension due to magnetostriction. Tsuya et al[7] developed a three terminal capacitive method to measure the magnetostriction of a stack of ribbons (sample) and this was further developed to measure the strain on a single ribbon by Ishio[8]. The magnetostriction cell used in their work was based on these devices and was built by Frank Jerems[9]. A schematic of their device is shown in Figure 1-5. One of the newer and simplest ways of measuring magnetostriction in the physics laboratory is by measuring the change in capacitance between a hollow cylindrical sample and a standard brass ring using a capacitance bridge meter, as previously developed in the WIU physics laboratory[10]. The work of this thesis was to standardize and to accurately calibrate this magnetostriction measurement device, verify its agreement with other earlier methods, and to improve the technique of fitting the data that it yields.

1-3. Magnetism

Any object which has the property of attracting iron and steel is known as a magnet. The mineral magnetite has this property of attraction in its natural state and is

Figure 1-5. O'Conner and Fawcett method of measurement of magnetostriction using a parallel plate capacitor. Figure is reprinted from Meas. Sci. Tech. 5 (1994).

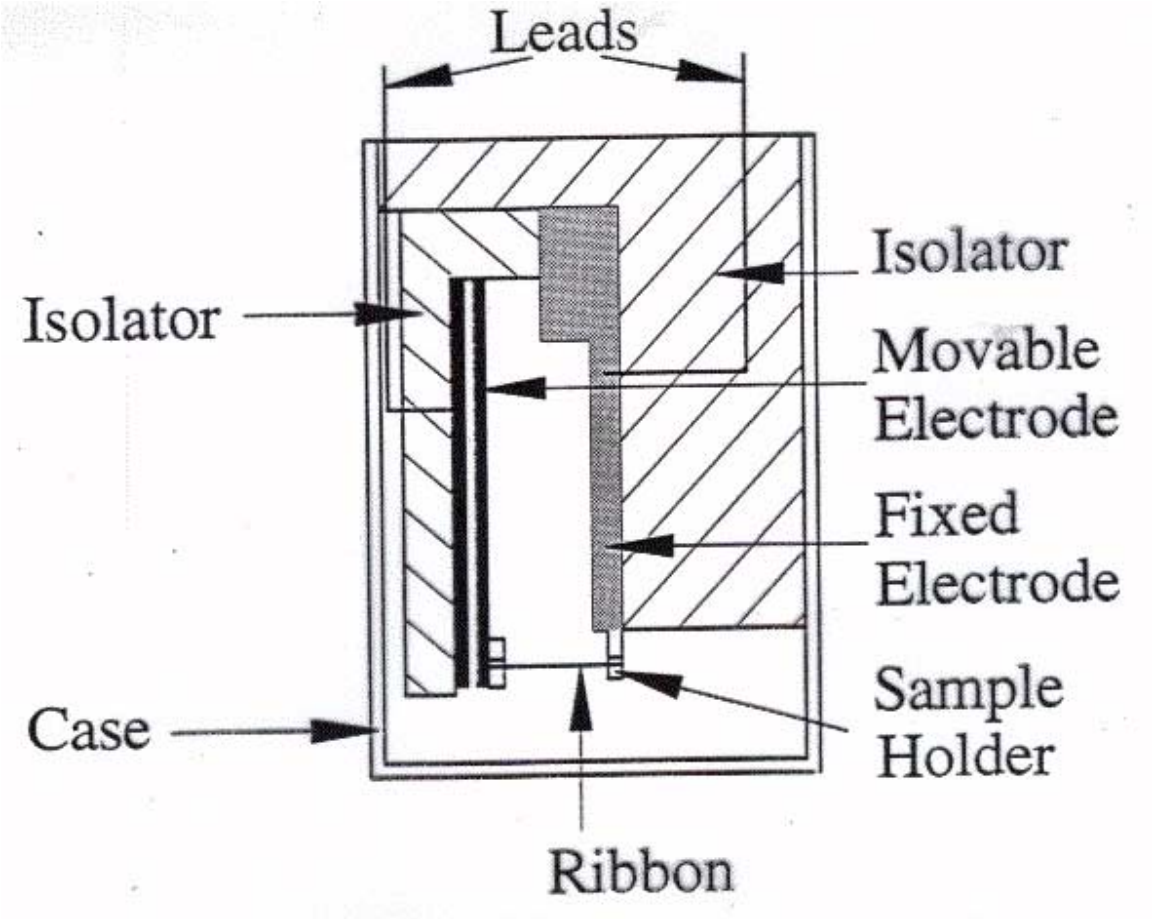

called a natural magnet. Magnetite was widely used during the middle ages to magnetize compass needles. Today natural magnets have less value as magnets because of their unstable physical structure and low magnetic strength. Better magnets can be made these days artificially from iron, nickel, cobalt, and their alloys, as well as from several rare-earth materials.

An early and one of the simplest theories of magnetism was the molecular theory. The molecular theory of magnetism states that a magnetic material is composed of a nearly infinite number of these molecular magnets. The molecules of an unmagnetized material are scattered so that they point in different directions, and this random placement causes the overall effect of these individual magnets to be neutralized.

Ampere, the great French physicist, discovered around 170 years ago that the magnetic moments are due to an electric current flowing in a circle whose plane is perpendicular to their direction. Since nothing was known about electrons at that time, Ampere could not explain how these currents occurred. It is now known to be the motion of electrons which generates the elementary magnetic force. In certain materials, these forces group together to form a magnetic domain. The fact that most materials are nonmagnetic is explainable by the assumption that the magnetic fields of individuals atoms cancel because of their random arrangements. However, magnetic materials such as iron, cobalt, nickel, and their alloys have a large permeability, and their arrangements are such that molecular moments enhance, rather than cancel each other.

Magnetism refers to the ability of the atomic magnets to be gradually forced into alignment by the influence of an external magnetic field. As shown in Figure 1-6, the

Figure 1-6. Electrons in the third orbit possessing unbalanced spins impart magnetism to an atom.

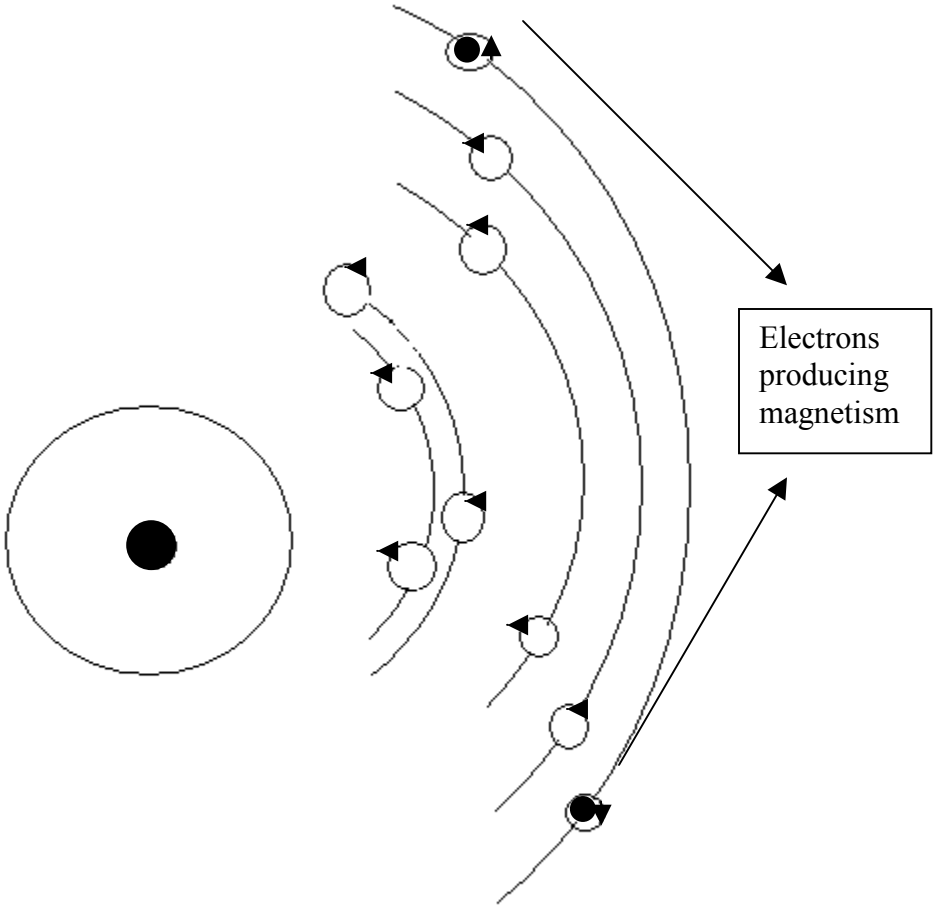

atoms of such materials contain a number of electrons (in the third ring) that possess uncompensated or unbalanced orbital spins. For example, an atom of iron shows an excess of four electrons with spin in one direction, cobalt has an excess of three, and nickel an excess of two. Unbalanced electron orbit spins create magnetic moments or magnetic twist, which imparts the characteristics of an electromagnet to the individual atoms. In nonmagnetic materials, the spins of all of the electrons cancel so that no net orbital spin or circulation of energy occurs.

1-4. Domain Theory

According to domain theory, charges in motion are the primary cause of a material's internal magnetism. The overall magnetism is the result of the planes of these spins in the individual atoms becoming aligned. The planes of these spins in ferromagnetic materials are brought into alignment by the application of an external magnetic field. The total magnetic induction of a ferromagnetic material then is created jointly by the externally applied field assisted by the molecular field. These molecular fields are called molecular domains and each domain exhibits parallel electron spins. Each domain of a ferromagnetic material contains on the order of 10^{15} atoms.

The domains in unmagnetized ferromagnetic materials are randomly oriented, but they can be rotated and eventually aligned almost completely with an externally applied magnetic field. This complete alignment occurs when magnetic saturation is reached and is also accompanied by the shifting of the domain boundaries themselves. The fundamental magnetic particle is therefore the electron, with its orbital and spin characteristics, but in most cases the magnetic effects of all the electrons in an atom can

nearly neutralize each other. This may cause the atoms in most cases to be slightly more magnetic (paramagnetic) or less magnetic (diamagnetic) than a vacuum.

1-5. Classification of Various Kinds of Magnetism

Substances which become magnetized when placed in a magnetic field are called magnetic substances. There are different kinds of magnetism, that is, differing moments per unit volume ($1m^3$) for magnetic substances, for which we use the symbol (M) in all cases to describe the intensity of this magnetization. The unit of M is Weber per square meter (Web/m^2). To describe the magnetization of a material, magnetic flux density or the magnetic induction (B) is also used. The relationship between the magnetic induction (B) and the intensity of magnetization (M) is given by

$$\mathbf{B} = \mathbf{M} + \mu_0 \mathbf{H} \tag{1.1}$$

where μ_0 is the permeability of free space, and the relationship between the intensity of magnetization M and the applied magnetic field (H) can be expressed as

$$\mathbf{M} = \chi \mathbf{H} \tag{1.2}$$

where χ is the magnetic susceptibility, for a material that is a linear magnetic material. The unit of χ is given as Henrys per meter, which is the same as that of μ_0. The relative susceptibility, χ_r, is then given by

$$\chi_r = \frac{\chi}{\mu_0} \tag{1.3}$$

where χ_r is a dimensionless number. From equations (1) and (2), we can then determine the magnetic induction (B) as follows

$$\mathbf{B} = (\chi + \mu_0)\,\mathbf{H}$$

$$\mathbf{B} = \mu\,\mathbf{H} \tag{1.4}$$

where the relative permeability μ_r can be expressed as

$$\mu_r = \frac{\mu}{\mu_0} \tag{1.5}$$

$$\mu_r = \chi_r + 1 \tag{1.6}$$

The observed value of relative susceptibility χ_r for weak magnetism is on the order of 10^{-5}, whereas for extremely strong magnetism it can be on the order of 10^5. For different magnetic structures the behavior of χ_r is different. Depending upon the behavior of χ_r the various kinds of magnetism are classified as:

i. Diamagnetism

ii. Paramagnetism

iii. Antiferromagnetism

iv. Metamagnetism

v. Parasitic ferromagnetism

vi. Ferrimagnetism

vii. Ferromagnetism

Most materials fall into one of these three categories or classifications:

i. $\chi_r < 0$ Diamagnetic Substance

ii. $\chi_r > 0$ Paramagnetic Substance

iii. $\chi_r \rightarrow \infty$ Ferromagnetic Substance

There are two possible atomic origins of magnetism which lead to the magnetization of a magnetic substance; orbital motion and the spin of the electron. An atom which has a magnetic moment caused by spin or by the orbital motion of electrons, or by both spin and orbital motion, is called a magnetic atom. The magnetic moments in materials such as nickel, cobalt, and iron are due to the spins of electrons.

Diamagnetism is a weak magnetism. In diamagnetic materials, the magnetization is in the opposite direction of the applied field. The relative susceptibility is negative and on the order of 10^{-5}. In paramagnetic materials, the magnetization **M** is directly proportional to the magnetic field **H**. The order of magnitude of relative susceptibility χ_r is on the order of 10^{-3} to 10^{-5} in this case, and it is positive. Paramagnetic materials contain magnetic moments caused by spin. Therefore, their magnetization can easily change direction. At very high temperatures the spins are thermally agitated and take random directions.

When an external magnetic field is applied across the paramagnetic substance, the average orientation of the spin is slightly changed, so that it produces a weak induced magnetization parallel to the applied magnetic field. The susceptibility in paramagnetic materials is inversely proportional to the absolute temperature, as shown in Figure 1-7(c), and magnetization M is directly proportional to the applied magnetic field (H). In the ferromagnetic case, the spins are aligned parallel to one another, in large scale domains of molecules. But when the temperature increases beyond the Curie point, the arrangements of spins in these materials becomes randomly distributed again due to thermal agitation. The Curie-Weiss law states that $1/\chi$ rises linearly with an increase in temperature from

Figure 1-7. Properties of paramagnetic materials are shown.

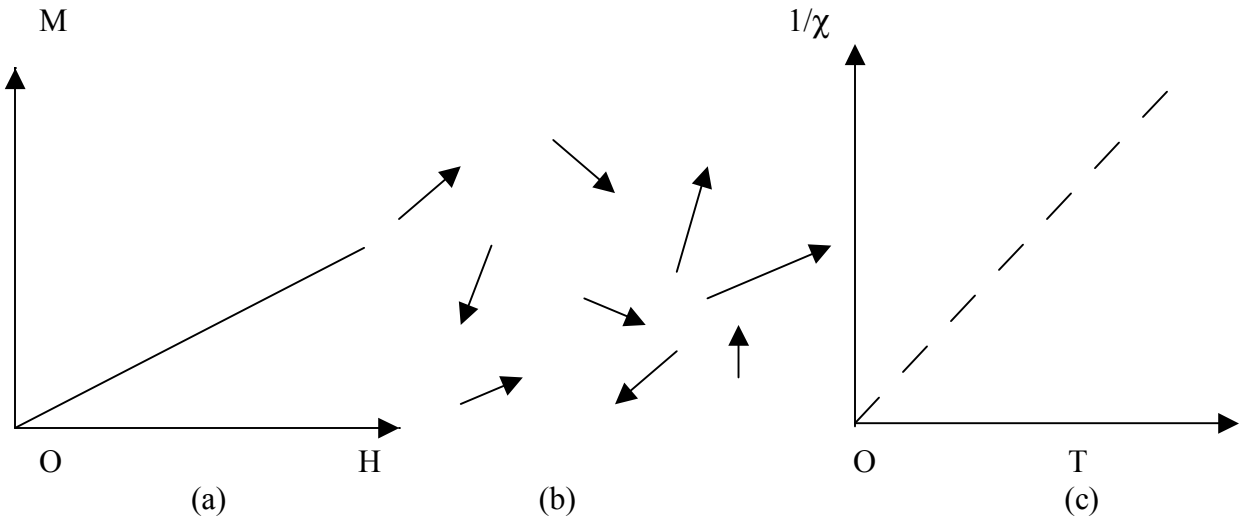

(a) The magnetization **M** is directly proportional to the magnetic field **H,** and the susceptibility (slope) is positive.

(b) Magnetic atoms or ions, whose spins are isolated from their magnetic environment, can more or less freely change their directions.

(c) The susceptibility in paramagnetic materials is inversely proportional to the absolute temperature.

zero at absolute zero temperature up to the Curie point. Most ferromagnetic substances are metals or metal alloys, with a few exceptions, such as oxides of Cr and Eu.

In spite of the frequent presence of spontaneous magnetization, a block of ferromagnetic substance in general is not magnetized but instead remains in a demagnetized state. This occurs because the inside of a ferromagnetic substance is divided into many magnetic domains, and whereas each magnetic domain is magnetized spontaneously, the overall direction of each individual domain is random. The magnetization of the block changes as shown in Figure 1-8. As the externally applied field increases, the magnetization of the block reaches the saturation level. When the external field is reduced, the magnetization of the sample also decreases, but it does not come back to the original value. Such an irreversible process of magnetization is called hysteresis. The magnetic saturation, the sample magnetization, and the amount of hysteresis as well as the hysteresis loop area, are the important characteristics for determining the suitable application of a particular ferromagnetic material (such as torque-sensing) as well as the parameters for these materials.

1-6. Hysteresis

One of the most important features of ferromagnetic substances is that they show a very complex change in magnetization when an external magnetic field is applied. This behavior is explained in Figure 1-9 where a typical hysteresis loop representative of a general ferromagnetic material is displayed.

At the origin where M = H = 0, i.e. the demagnetized state, as the field is increased the magnetization increases along the curve OABC and finally reaches the

Figure 1-8. This is a typical magnetization curve for a ferromagnetic substance.

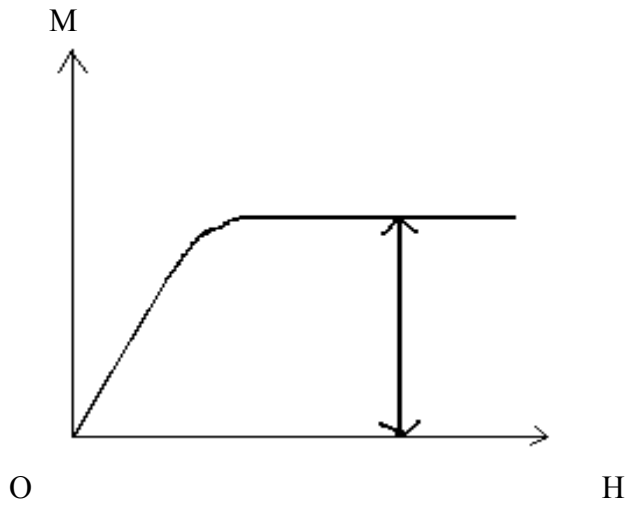

Figure 1-9. The initial magnetization curve and minor loop is shown for a typical ferromagnetic material.

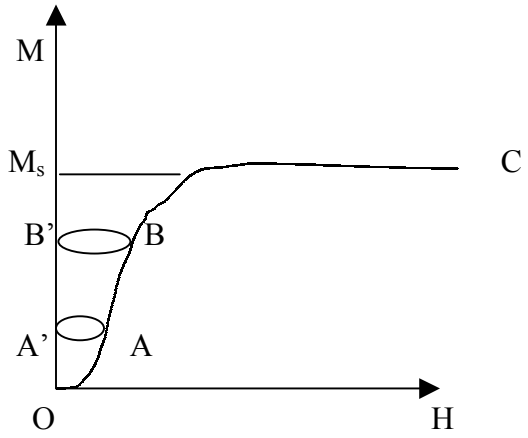

saturation magnetization (M_s). The inclination of the curve OA is called the initial susceptibility. In region OA the process of magnetization is clearly still reversible. That is, when the field is reduced to zero the magnetization reduces back to zero as well. Beyond the region OA the process becomes irreversible. If the magnetic field is decreased from point B, the magnetization will not follow the same path but will instead follow BB'. The inclination of BB' is called the reversible susceptibility χ_{rev} or the incremental susceptibility. The slope of the initial magnetization curve OABC is called the differential susceptibility χ_{diff}, and the slope of a line which connects the origin O and each point of the initial magnetization curve is called the total susceptibility $\chi_{tot.}$ The change in χ_{rev}, χ_{diff}, and χ_{tot} along the initial magnetization curve are shown in Figure 1-10. If the magnetic field is decreased from the saturated state C as shown in Figure 1-11, the magnetization **M** decreases along the path CD and not along the path CBAO.

At H = 0 it reaches some finite value M_r, known as the retentivity, or the remanence, or the remanent magnetization of the material (OD). Furthermore, applying the negative or reversed magnetic field causes the intensity of the magnetization to still further decrease until it finally again reaches zero intensity. The field at this point is called the coercive force H_c (OE), and the portion DE of the magnetization curve is called the demagnetization curve. Further increase of H in a negative sense or in the reverse direction then results in an increase of the intensity of the magnetization in the negative sense or in the reverse direction, and finally leads to a negative saturation magnetization. When the field is reversed again to the positive sense the magnetization will change along FGC to a remanence in the reverse orientation. The closed loop CDEFGC is called a

Figure 1-10. Various kinds of magnetic susceptibilities are plotted as functions of the intensity of magnetization.

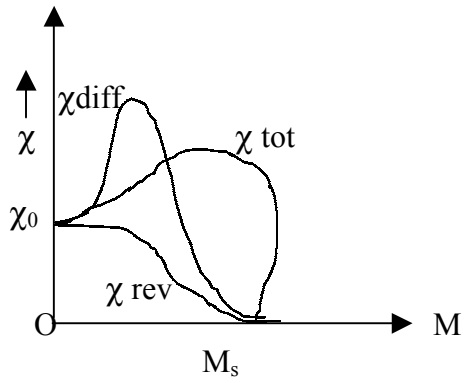

Figure. 1-11 A typical ferromagnet's hysteresis loop is displayed.

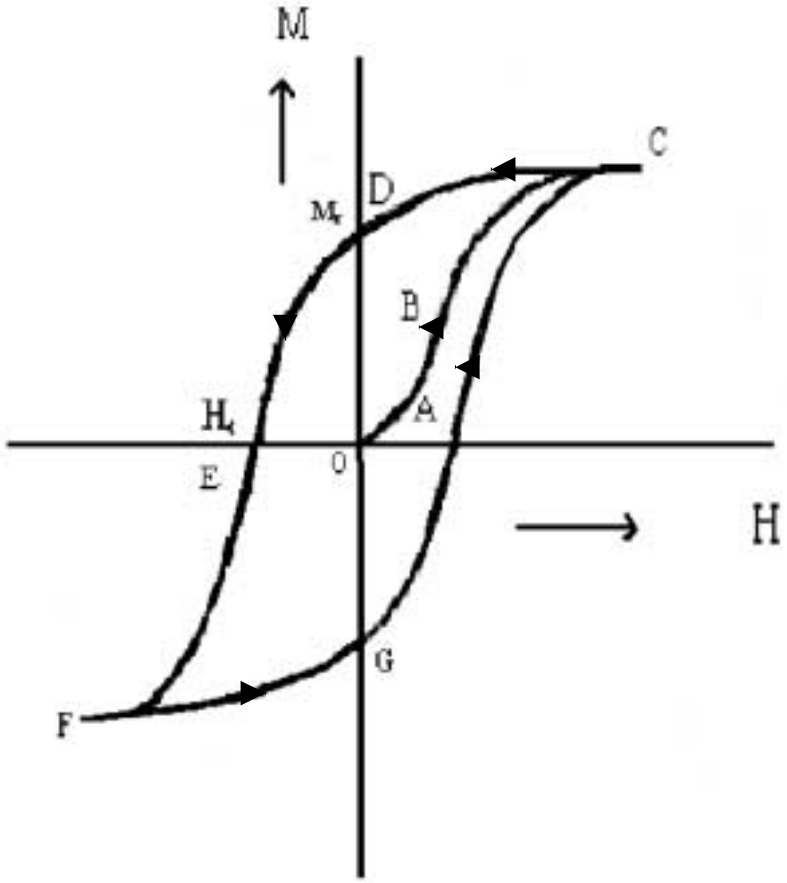

hysteresis loop. The work required to magnetize a unit volume of a cylindrical ferromagnetic substance from M_1 to M_2 is given by

$$W = \int_{M1}^{M2} HdM \tag{1.7}$$

By putting $M_1 = 0$ and $M_2 = M_s$, the work required to magnetize the volume from a demagnetized state to a saturation state M_s can be calculated. This work is equal to the area surrounded by the ordinate axis, the line $M=M_s$ and the initial magnetization curve as shown in Figure 1-12. The energy supplied by this work is partially stored as potential energy, and also partially dissipated as heat, which is generated in the substance. During one complete cycle of the hysteresis loop the potential energy should return to its original value; therefore, the resultant work would be consumed as heat. This heat is called the hysteresis loss and is given by

$$W_h = \oint HdM \tag{1.8}$$

which is equal to the area contained within the hysteresis loop, that is, within the M-H or the B-H graph. Ferromagnetic substances, which have high permeability, low coercive force, and small hysteresis are classified as soft magnetic materials; whereas hard magnetic materials have high coercivity, high remanence, and large hysteresis loss. Soft magnetic materials are used for iron cores of transformers, motors, and generators. Hard magnetic materials are used as permanent magnets for various kinds of electric motors, loud speakers, and any other types of apparatus for which high remanence or high coercivity would be desirable. As a result of the development of magnetic materials, the

Figure 1-12. The work required to saturate a unit volume of a ferromagnetic substance is shown in the shaded region.

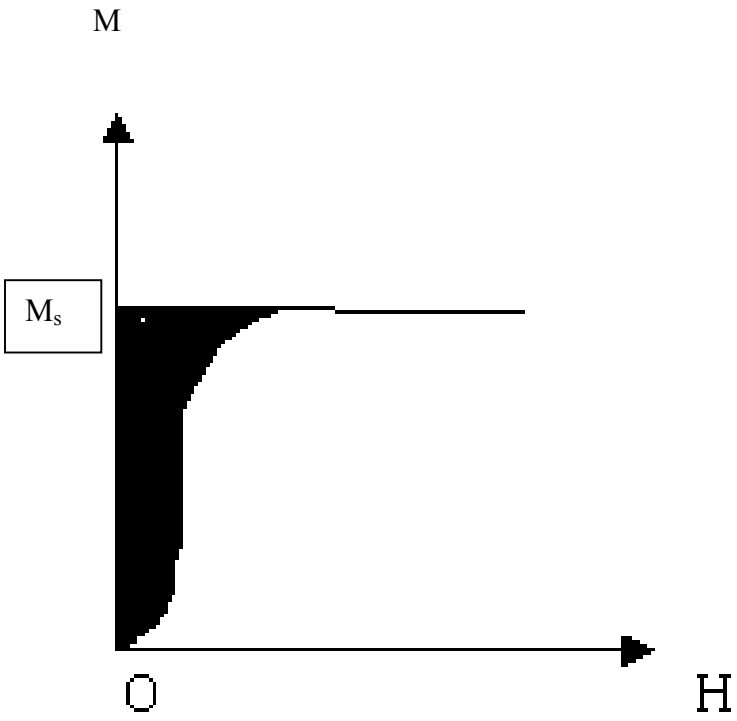

characteristics of existing magnetic materials cover a wide range from extremely soft to extremely hard materials magnetically.

In the beginning of the twentieth century, soft iron was used as a soft magnetic material. This substance has a hysteresis loop which is very wide compared to that of permalloy. One of the typical soft magnetic materials is shown in Figure 1-13. Similarly, a carbon steel which was used as a permanent magnet until the beginning of the twentieth century has a hysteresis loop narrow compared to that of an MK magnet which is one of the typical present-day permanent magnetic materials as shown in Figure 1-14. Various hysteresis constants are listed in Table 1-1 for several typical magnetic materials.

Figure 1-13. A comparison is made for hysteresis curves of soft iron and permalloy.

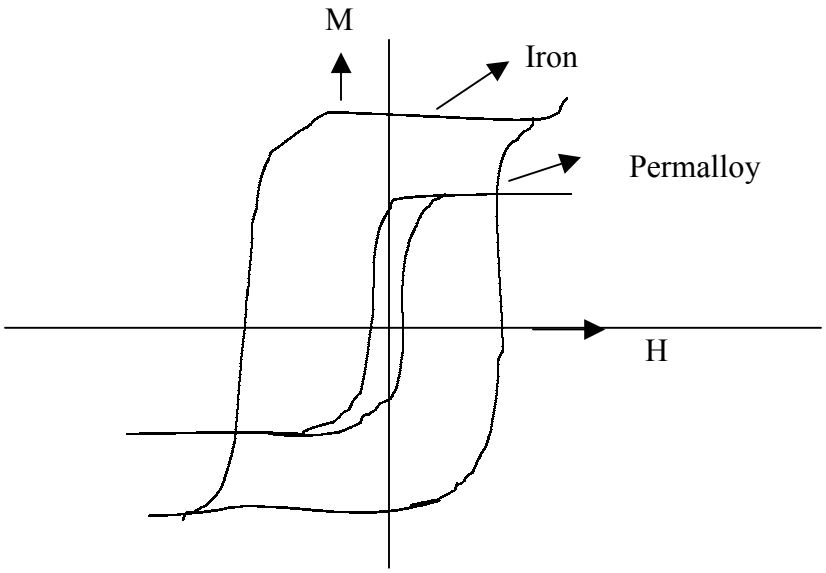

Figure 1-14. A comparison is made for hysteresis curves of carbon steel and MK steel.

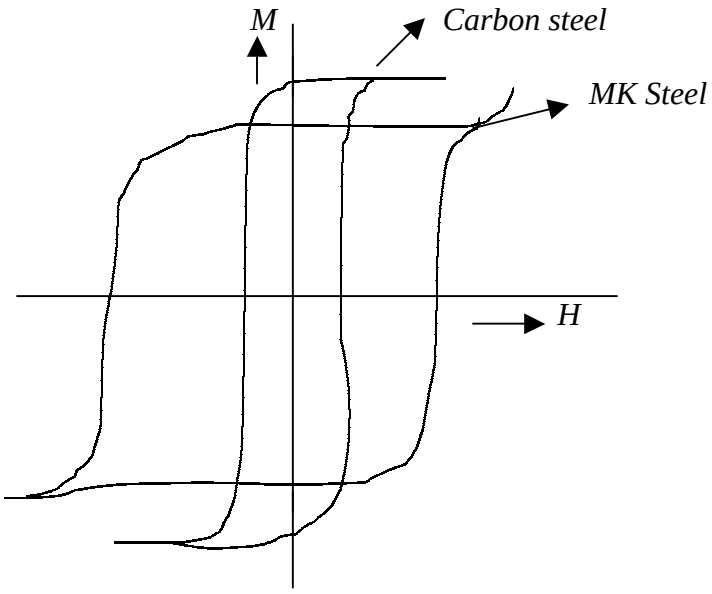

Table 1-1. Magnetic Properties of Some Magnetic Materials (Bozorth[11]).

Material	**Remanence**	**Coercive Force**
	Wb/m^2	Oe
Mild steel	2.12	1.8
78 permalloy	1.08	0.05
Cobalt	1.79	10
Nickel	0.69	0.7
Steel 4340[12]	1.23	38

Chapter 2. Theory

2-1. Curie's Law

In 1895 Curie showed that a certain class of substances had temperature dependent and field independent susceptibilities. The susceptibility for these materials is given by

$$\chi = \frac{C}{T} \tag{2.1}$$

where T is the absolute temperature and 'C' is called Curie's constant [13]. This conclusion was based on studies of oxygen gas (O_2), of the solutions of some salts, and of some ferromagnetic metals at temperatures above a critical value, known as the Curie temperature. Substances that obey Curie's law are known as paramagnets. The type of susceptibility observed by Curie is now known to occur only for substances that contain permanent magnetic dipoles. Later experiments showed that not all paramagnetic materials obey Curie's law. Some materials have susceptibilities that obey the equation

$$\chi = \frac{C}{T - \theta} \tag{2.2}$$

where 'θ' is a constant. This equation is known as the Curie-Weiss law and is based on a classical theory developed by Weiss. Atoms or ions of the transition group elements, or ions isoelectronic with these elements, form the largest class of substances to obey the Curie or the Curie-Weiss law. These elements have permanent moments because of

uncompensated electrons in an inner shell. The rare earth ions when present in solution, or in a solid salt, usually give rise to this type of paramagnetism.

2-2. The Effect of the Crystalline Field

Generally paramagnetic ions in solids and in solutions have been considered as though they are free. But they are in fact acted on by the inhomogeneous electric fields that are produced by their diamagnetic neighbors. The effect of these fields on the rare earth ions at ordinary temperatures is very small, so that the ions behave as though they are free. In the ions from the iron-group of the periodic table, where electrons are responsible for the paramagnetism, the 3-d shell electrons will be affected by the crystalline fields to a much greater degree. This is partly due to the large radius of the 3-d shell and partly due to the lack of any outer electronic shells to screen the 3-d shell. The general effect of the crystalline field is to cause some splitting of the otherwise degenerate energy levels. The precise value of the electric field cannot be calculated by theory, since the charge distribution of the diamagnetic neighbors and the overlapping of the electrons clouds are difficult to determine.

2-3. Magnetic Anisotropy

Magnetic anisotropy is the dependence of the internal energy on the direction of spontaneous magnetization. This type of energy term is known as the magnetic anisotropy energy. Generally, the magnetic anisotropy energy term contains and depends on information about the crystal symmetry of the materials, and it is therefore called the crystalline magnetic anisotropy. By applying mechanical stress to the material, as in the

Sixtus-Tonks experiment[14], which will be explained in the next section, the magnetic anisotropy can then be observed. We can also control the magnetic anisotropy by heat treating the material in a magnetic field or by cooling it in a controlled manner. This is called the induced magnetic anisotropy.

2-4. Sixtus-Tonks experiment

In 1931 Sixtus and Tonks[15] succeeded in obtaining a large magnetic domain by stretching a thin long permalloy wire. Generally, a crystal of ferromagnetic substance is spontaneously deformed along the direction of internal magnetization. In the case of permalloy wire, when the tension is applied along the length of the wire, the internal magnetization will point parallel or antiparallel to the axis of the wire, so as to produce an additional elongation in the direction of the external tension. After magnetizing the wire in one direction, Sixtus and Tonks applied a reverse field, and then they observed the motion of the domain boundary created by the starting coil C_2 as shown in Figure 2-1. They measured the velocity of its propagation by observing the time interval between the two signals induced in the search coils S_1 and S_2. This phenomenon is known as the large Barkhausen effect. In 1932 Bloch[16] showed theoretically that the boundary between magnetic domains is not sharp on an atomic scale, but is spread over a certain thickness in which the direction of electronic spins or molecular moments changes gradually from one domain to the next. This layer of changing moments is usually called a domain wall or a Bloch wall.

Figure 2-1. A schematic diagram of the Sixtux-Tonks experiment is reprinted from The Physical Principle of Magnetism[17](1931).

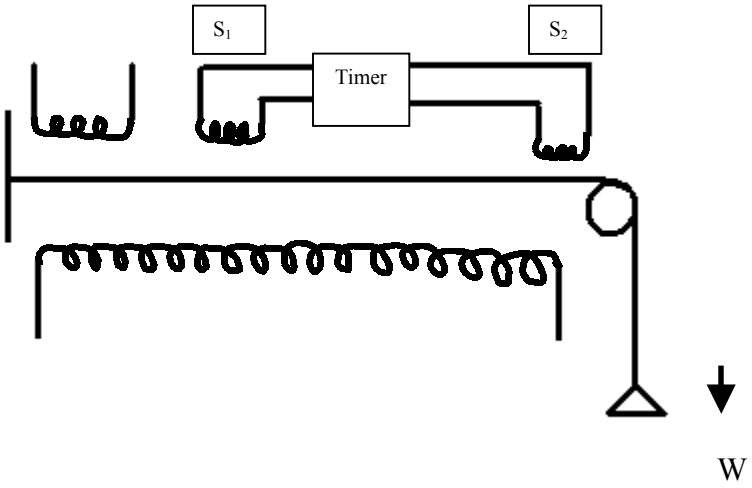

(a)

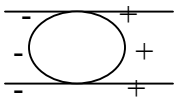

(b)

(a) The experimental arrangement of the Sixtus-Tonks experiment is shown.

(b) An island of reverse magnetization is shown.

2-5. Single Crystal anisotropy

Most of the older measurements of magnetic susceptibility have been made on powders or polycrystalline solids. When a single crystal is employed, anisotropic behavior will occur provided the crystalline field lacks spherical symmetry. Then the electronic orbits will be distorted along particular directions, and the resulting magnetization will depend on the direction of an externally applied magnetic field. It is obvious that measurements on single crystals give valuable information on the symmetries of the crystalline field.

2-6. Mechanism and Origin of Magnetostriction

The phenomenon of magnetostriction originates in the interaction between the atomic magnetic moments. The origin of magnetostriction along the lines of Neel's theory [18] was developed in his paper on magnetic annealing and surface anisotropy. When the distance between the atomic magnetic moments is variable, the interaction energy is expressed as [19]

$$w(r,\cos\phi) = g(r) + l(r)(\cos^2\phi - \frac{1}{3}) + q(r)(\cos^4\phi - \frac{6}{7}\cos^2\phi + \frac{3}{35}) + \ \ldots \ (2.3)$$

where r is the interatomic distance as shown in Figure 2-2. If the interaction energy is a function of 'r', the crystalline lattice must be deformed upon the generation of a ferromagnetic moment, because such an interaction tends to change the bond length in a different way depending on the bond direction. The first term, g(r), is the exchange

Figure 2-2. A typical magnetic dipole pair is shown.

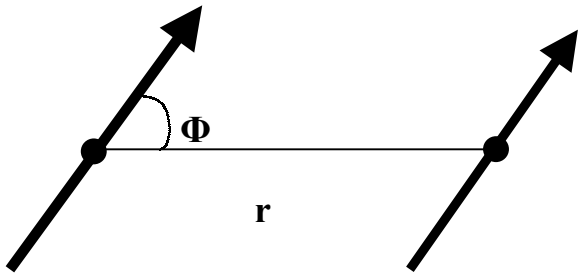

interaction term. It is independent of the direction of magnetization. Thus, the crystal deformation caused by the first term does not contribute to the usual directional magnetostriction, but it does play an important role in the volume magnetostriction effect. The second term, l (r), represents the dipole-dipole interaction, which depends on the direction of magnetization, and is usually the main origin of the observed directional magnetostriction. The remaining terms that follow normally lend a small contribution as compared to this second term. Therefore the higher order terms may be safely neglected. So, the pair energy can be expressed as

$$w(r,\phi) = l(r)(\cos^2\phi - \frac{1}{3}) \tag{2.4}$$

If we then let $(\alpha_1,\alpha_2,\alpha_3)$ denote the direction cosines of the domain magnetization and we let $(\gamma_1,\gamma_2,\gamma_3)$ be those of the bond direction, then equation 2.4 becomes

$$w = l(r)[\cos(\alpha_1\gamma_1 + \alpha_2\gamma_2 + \alpha_3\gamma_3)^2 - \frac{1}{3}] \tag{2.5}$$

Finally, for a polycrystalline material like our samples, the longitudinal magnetostriction is calculated by averaging for all different crystalline orientations by assuming $\alpha_i = \beta_i$ for i = 1, 2, and 3, giving

$$\frac{\Delta l}{l} = \lambda(\cos^2\theta - \frac{1}{3}) \tag{2.6 a}$$

where λ is the isotropic magnetostriction, which has replaced l (r). In our case, only the 2 dimensions of the circumference are considered, since the effect of the change in length of the inner ring on the capacitance is negligible. Therefore we obtain

$$\frac{\Delta l}{l} = \frac{2}{3}\lambda(\cos^2\theta - \frac{1}{3}) \qquad (2.6\text{ b})$$

In these equations, 'θ' is now the angle between the direction of the domain and that of the observation. It can be noted that the final form of the magnetostriction is the same as that of the isotropic magnetostriction, $e = \frac{\Delta l}{l}$, where 'e' is the elongation in the direction of magnetization. If the elongation of the sample is not in the same direction as the applied magnetic field and it makes some angle 'ϕ' with the direction of magnetization as shown in Figure 2-3, then the magnetostriction is given by

$$\frac{\Delta l}{l} = e\cos^2\Phi \qquad (2.7)$$

2.7 Sample Ring

In order to measure the magnetostriction of a ferromagnetic material, a double ring technique was recently (2000) introduced at Magnalastic Devices, Incorporated (MDI)[21]. For this technique, two rings of the same material are shrink-fitted together. Because the inner ring is compressed, and the outer ring is under tension, they both have a large "hoop stress". This causes all the domains of the inner ring to be axially aligned. Then the application of an external magnetic field in the circumferential direction will align all of the domains in the double rings circumferentially, thus demonstrating the magnetostriction effect due to the inner ring. Although the measurement of magnetostriction using the double ring technique is more accurate than that of a single ring due to previous knowledge of domain orientation, it is very difficult and complex to prepare the sample. Additionally, for the measurement of the change in capacitance, the electrical circuit used by MDI

Figure 2-3. The elongation is observed in a direction which makes an angle φ with the axis of spontaneous strain.

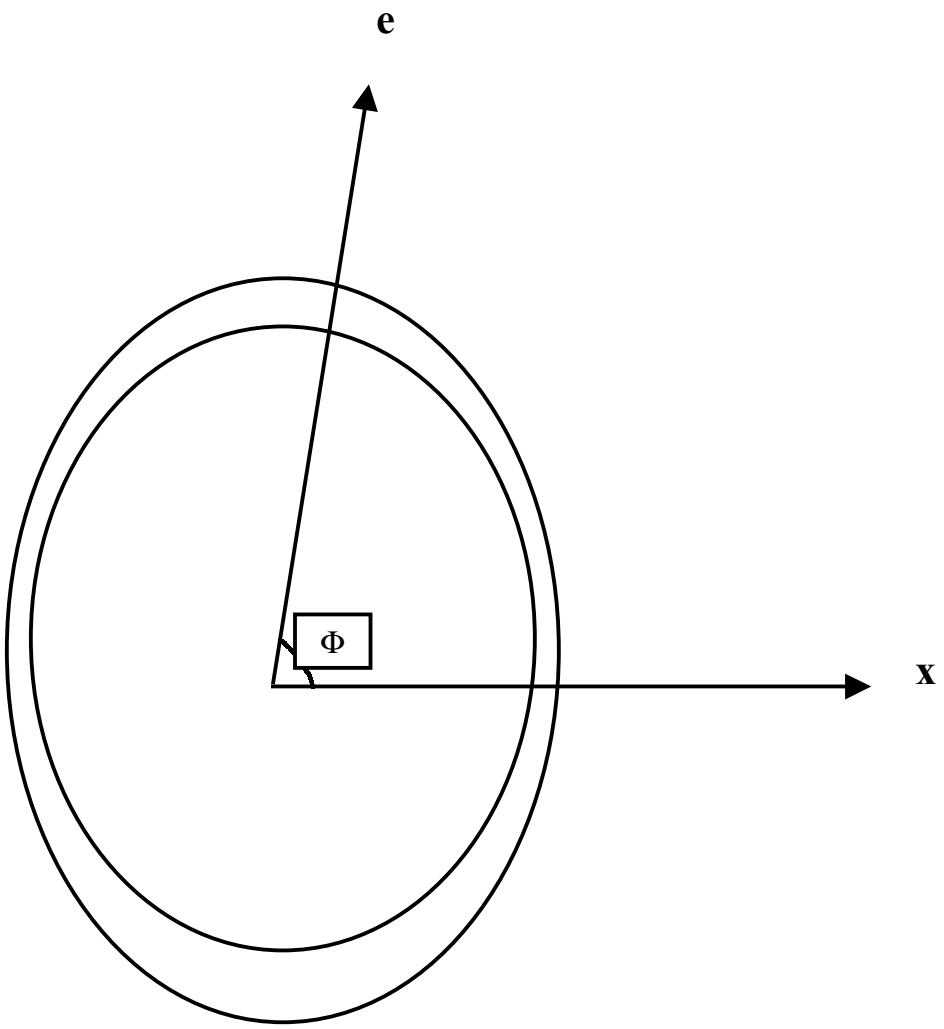

required very expensive crystal oscillators and interference devices that were complex to assemble. In our WIU physics laboratory, we have developed a simple, cost-effective single ring method to measure magnetostriction. The mechanism of magnetostriction at an atomic level is relatively complex subject matter, but on a macroscopic level it may be separated into two distinct processes. The first process is dominated by the migration of domain walls within the material in response to external magnetic fields, and the second process is dominated by the rotation of the domains. In this method we used two rings of different diameter as shown in Figure 2-4. The outer ring used is a fixed diameter brass ring that will demonstrate no magnetostriction effect, while the inner ring is the sample ring. These two rings act as a cylindrical capacitor, which is a measure of the capacity to store charge for a given potential difference, so that by measuring the change in capacitance when the external circumferential magnetic field is applied, expansion or contraction due to magnetostriction can be calculated.

The single ring technique that we used is not very different than the double ring. In single ring measurements the level of magnetostriction is approximately half the double ring level. This can be compared to the principle of polarization. As shown in Figure 2-5 the incident light can be compared to the direction of domains in the double ring. Thus, let the beam of light 1 correspond to the circumferential direction of domains, and the beam of light 2 correspond to the axial direction of domains, and the beam of light 3 is the random direction of domains, which corresponds to the single ring. Note that the single ring will yield about half the magnetostriction level of the double ring as in the polarization case; when a polarization sheet is placed in either the horizontal or vertical direction, the intensity

Figure 2-4. (a) Diagram of our two sample rings, when there is no magnetic field applied.

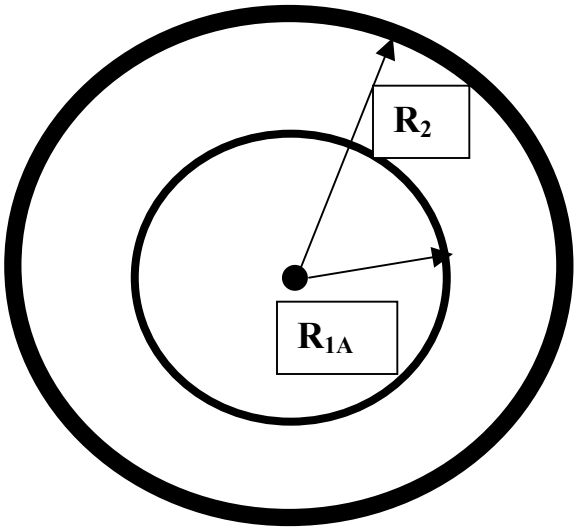

(b) When there is a magnetic field applied, this introduces a change in the outer radius of the inner ring.

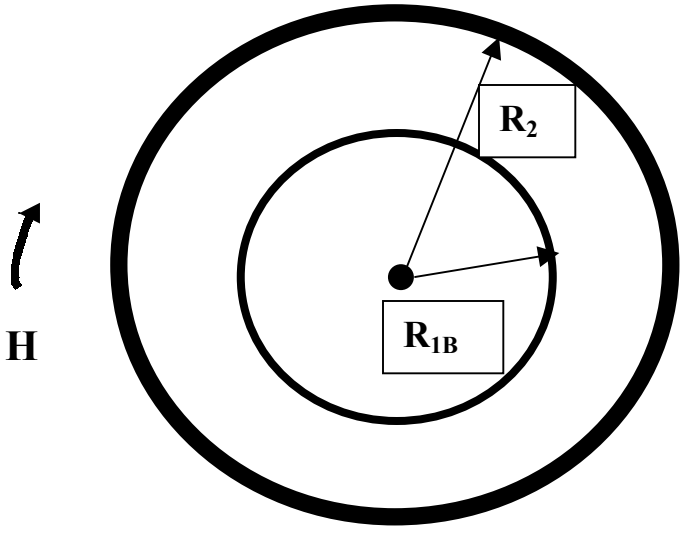

Figure 2-5. The polarized film transfers 100% for the same directional light, 0% for the perpendicular light, and 50% for the random directional light. This figure is reprinted from the M.S. thesis by Won-Chul Shin, under Dr. Boley's advisement in the WIU Physics Department.

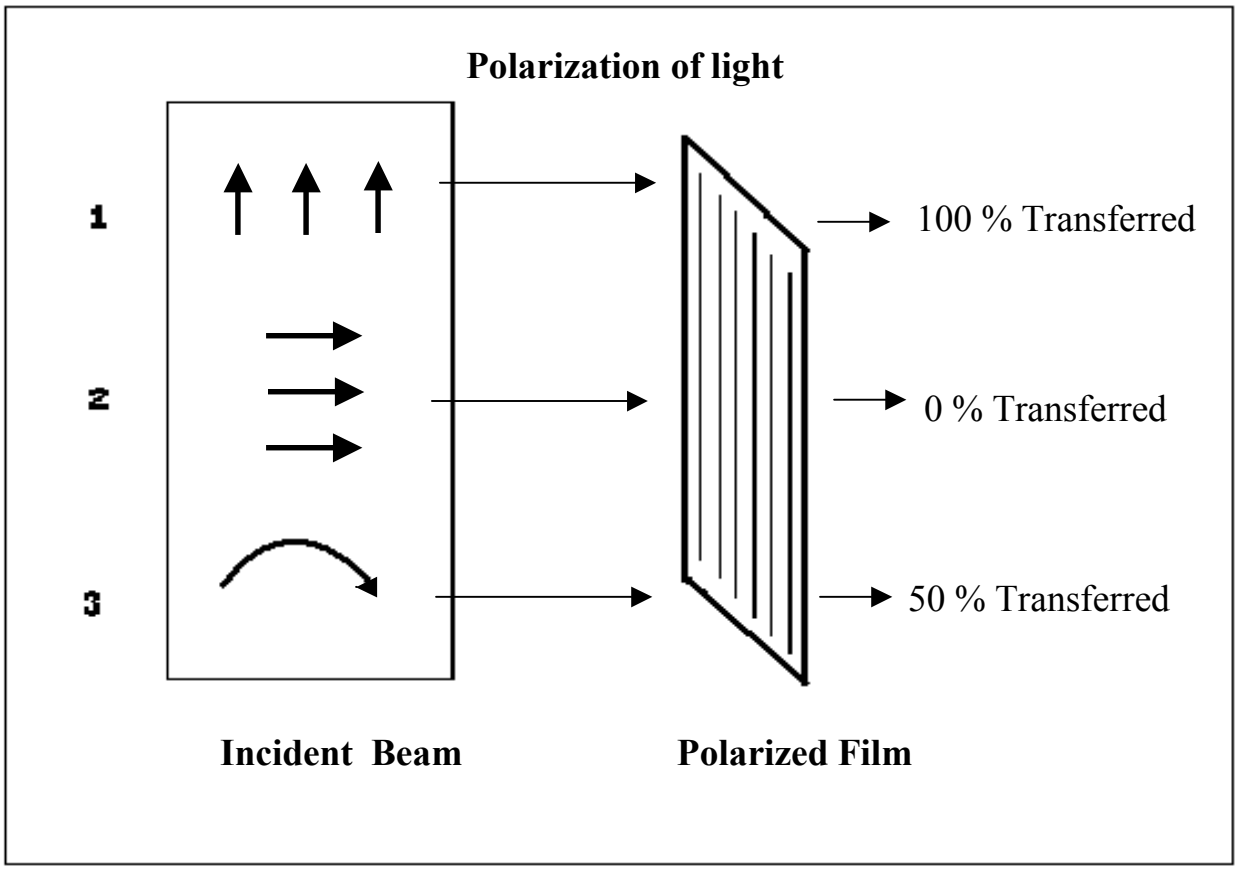

of the random polarization beam becomes only half the intensity of the original beam. However, with the same polarization sheet, light aligned with the axis of the sheet would have experienced almost 100% transmission of the original intensity. This 50% effect occurs because in the single ring technique there is no "hoop stress" to orient the domains in one favorable direction, so they maintain random directions. This can be further shown by using the law of Malus[22] which states that the intensity of the transmitted beam, I_t, in terms of the intensity of the incident beam, I_i, is given by

$$I_t = I_i Cos^2\phi \tag{2.8}$$

the average intensity I_{ave} can be obtained by integrating the equation (2.8) over one half of the period. This yields the result:

$$I_{ave}\pi = \int_0^{\pi} Cos^2\theta d\theta = (\frac{\theta}{2} + \frac{1}{4} Sin2\theta)$$

or,

$$I_{ave}\pi = \frac{\pi}{2} \tag{2.9}$$

and, therefore, the average intensity, $I_{ave,}$ would be

$$I_{ave} = \frac{1}{2} \tag{2.10}$$

Just as in this concept of polarization, our value of magnetostriction should also be approximately half the observed value in the double ring measurement as conducted by MDI for the 4340 steel as well as approximately half the printed value of magnetostriction in Bozorth for nickel and iron, as obtained from earlier magnetic experiments.

2-8. Cylindrical Capacitance Arrangement

A cylindrical capacitor consists of two conducting cylinders of radius R_1 and R_2 respectively, and of length 'L', with a charge +Q on the inner conductor and a charge –Q on the outer conductor. The electric field outside of the inner cylinder of charge Q and radius R_1 is given by

$$E_r = \frac{\lambda}{2\pi\varepsilon_0 r} \qquad \text{(with } r > R_1\text{)}$$

$$= \frac{Q}{2\pi\varepsilon_0 Lr} \tag{2.11}$$

where $\lambda = \frac{Q}{L}$ is the linear charge density on either cylindrical conductor. The field due to – Q on the outer cylindrical shell is zero inside the shell, for $r < R_2$, which can be easily shown using Gauss's Law, since there is no enclosed charge. The potential difference 'V' between the conductors is then found using the following equation:

$$V = V_+ - V_- = V_{R_{1A}} - V_{R_2}$$
$$V = -\int_{R_2}^{R_{1A}} \vec{E} \cdot d\vec{r}, \tag{2.12}$$

$$= -\frac{Q}{2\pi\varepsilon_0 L}\int_{R_2}^{R_{1A}}\frac{dr}{r}$$

$$= \frac{Q}{2\pi\varepsilon_0 L}\int_{R_{1A}}^{R_2}\frac{dr}{r} = \frac{Q}{2\pi\varepsilon_0 L}\ln\frac{R_2}{R_{1A}} \qquad (2.13)$$

where R_{1A} is the radius of the sample ring when there is no magnetic field applied. The potential on the inner conductor is higher than that of the outer conductor, since the electric-field lines point from the inner conductor to the outer conductor.

Thus the potential difference for the capacitor is given by

$$V = \frac{Q\ln(\frac{R_2}{R_{1A}})}{2\pi\varepsilon_0 L} \qquad (2.14)$$

and the capacitance is given by

$$C_1 = \frac{2\pi\varepsilon_0 L}{\ln(\frac{R_2}{R_{1A}})} \qquad (2.15)$$

The capacitance is proportional to the length of the conductors. The greater the length, the greater the amount of charge that can be put on the conductors for a given potential

difference, since the electric field, and therefore the potential difference, depends only on the charge per unit length. When a strong magnetic field is applied, the inner radius of the sample ring changes to radius $R_{1B,}$ due to the magnetostriction effect. The changed capacitance C_2 can then be calculated from

$$C_2 = \frac{2\pi\varepsilon_0 L}{\ln(\frac{R_2}{R_{1B}})} \tag{2.16}$$

where R_{1B} is the radius of the sample ring when there is an applied magnetic field and the magnetostriction effect is occurring.

From equations (2.16) and (2.17), we can now obtain the ratio of the new to the old capacitance (in- field value ratioed to the zero-field value):

$$\frac{C_2}{C_1} = \frac{\ln R_2 - \ln R_{1A}}{\ln R_2 - \ln R_{1B}} \tag{2.17}$$

where solving for R_{1B}, yields the result:

$$R_{1B} = \exp[\ln R_2 - \frac{C_1}{C_2}(\ln R_2 - \ln R_{1A})] \tag{2.18}$$

The magnetostriction is given by the ratio of the change in the circumferential length ‘ Δl’ to the original length ‘l’, where this original ‘l’ would be given by $2\pi R_{1A}$ and the new l'

given by $2\pi R_{1B}$. Thus the fractional change in length, or the magnetostriction, would be determined from

$$\frac{\Delta l}{l} = \frac{l' - l}{l} = \frac{R_{1B} - R_{1A}}{R_{1A}} \tag{2.19}$$

Substituting the R_{1B} from equation (2.19) to equation (2.20) we can now obtain:

$$\frac{\Delta l}{l} = \frac{\exp[\ln R_2 - \frac{C_1}{C_2}(\ln R_2 - \ln R_{1A})] - R_{1A}}{R_{1A}} \tag{2.20}$$

The new capacitance, C_2, is the sum of the original capacitance, C_1, and the change in capacitance, ΔC, which is observed as a result of the application of the external magnetic field, that is,

$$C_2 = C_1 + \Delta C \tag{2.21}$$

Substituting C_2 to equation (2.21) and letting C_1= C, the original capacitance, we obtain the final formula for the measured magnetostriction, $\frac{\Delta l}{l}$, as follows:

$$\frac{\Delta l}{l} = \frac{\exp[\ln R_2 - \frac{C}{C + \Delta C}(\ln R_2 - \ln R_{1A})] - R_{1A}}{R_{1A}} \tag{2.22}$$

This formula is programmed into our Microsoft Excel spreadsheet, and by plugging in the values of R_2, C, and $R_{1A,}$ which are fixed for each sample, and ΔC which is to be measured in each experiment, we can then obtain the value of magnetostriction, $\frac{\Delta l}{l}$, in parts per million (ppm).

Chapter 3. Experimental Setup

3-1. Experiment

The diagram of our experimental setup is shown in Figure 3-1. The first block from the top left is an AC welder power supply, used for the input of a large 60 Hz current. The second block in the diagram is the shunt (a standard low resistance) connected parallel to the X-channel of the storage oscilloscope to avoid damaging the CRO because of the high current of over 500 Amperes generated by the welder power supply. The standard resistance of the shunt, S, is calculated by using Ohm's Law.

$$S = V / I = 100 \text{ V} / 500 \text{ A} = 0.0002 \text{ Ohm}$$

Thus, this shunt produces a 1V signal for every 5A of current passing through it. This shunt is also then used to give the X-channel of the CRO a voltage signal proportional to the current level produced by the welder power supply. The third block in the diagram is the sample holder, made of Teflon. It stabilizes the brass ring, which forms the outer plate of the cylindrical capacitor. The Teflon sample holder also allows the copper rod to go down through its center to carry the large supply current. A sample ring is put inside the brass ring, and the two rings are separated by rubber washers at the ends to prevent their being shorted out during the experiment as well as to hold their spacing constant. A copper rod was used to pass the current through the sample ring instead of a welding rod. The copper rod allows for the passage of the maximum current levels with minimal power dissipation, since the copper rod has very low resistance. A traditional welding rod would have high resistance, which would dissipate more heat, causing thermal expansion in the sample and errors in the measurements, as well as severely limiting the

Figure 3-1. This is the schematic diagram of our laboratory setup for magnetostriction measurements.

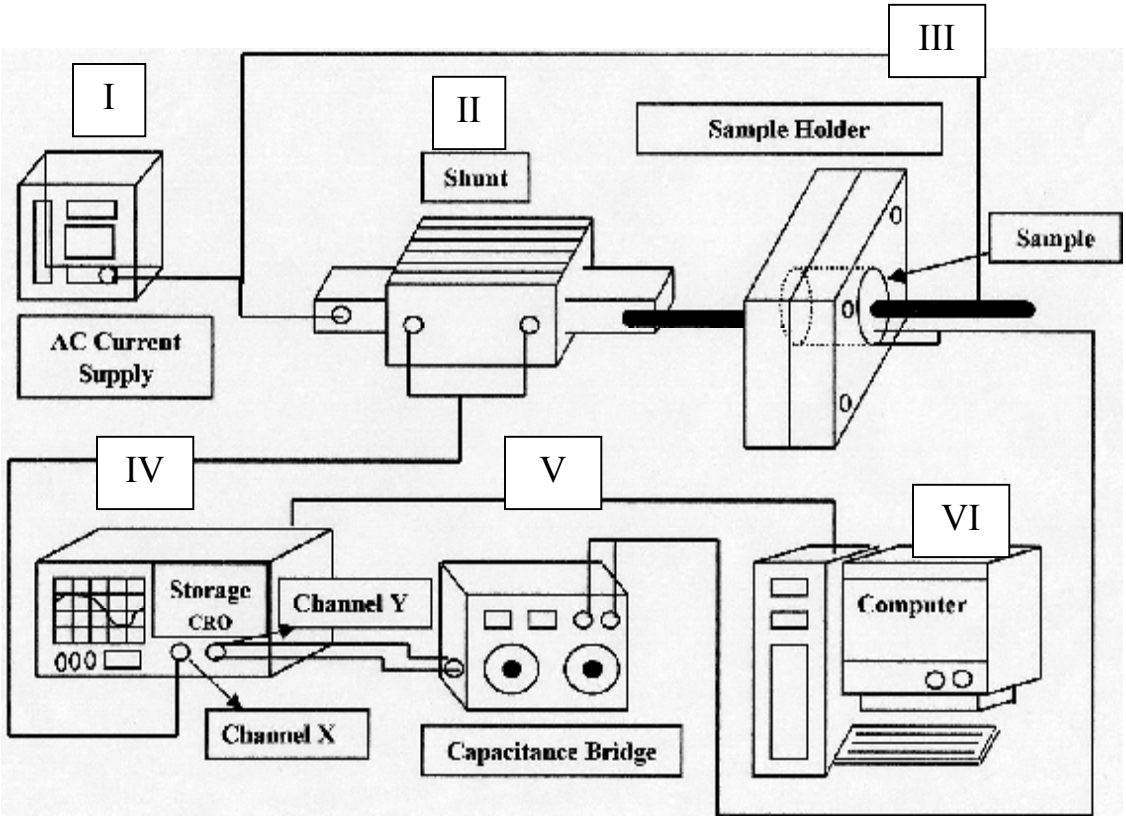

maximum current value we would reach in our experiments. The fourth block in the diagram is the CRO. The 'X' channel of the CRO is used to store the data from the input voltage V(t), which is used later to convert to the magnetic field, H(t). The 'Y' channel stores the data from the capacitance bridge meter, which is later used to calculate the change in capacitance, $\Delta C(t)$. The fifth block is the capacitance bridge meter. It measures the change in capacitance by showing the deflection away from the null point after it has been zeroed with the base capacitance value before the application of the high levels of current and field. Finally the sixth block in the diagram is that of the Gateway computer with its GPIB interface board, which has a Graphic language, LabView. The LabView program was used to receive the data from the storage CRO, which was analyzed further to calculate the change in the sample capacitance due to magnetostriction effects.

3-2. Sample Construction

The most important part of this experiment is to prepare the sample rings with extremely precise tolerances. The steel rings (samples) were constructed in our WIU machine shop last year with the help of Mr. Edgar Wendell Hoover and an undergraduate physics major, Daniel K. Pratt. The nickel and iron rings were made this year with the help of Jason Wilson, an undergraduate physics major. Two steel rings, of materials 4620 and 4340, which are ferromagnetic and have different nickel compositions, were used. The other three samples we used were of aluminum, nickel and iron. The internal radii of the 4340 ring, 4620 ring, aluminum ring, nickel ring, and iron ring were 8 mm, 8.05 mm, 8 mm, 7.66 mm, and 7.82 mm, respectively, and the external radii, R_{1A}, when

there was no current passing through the copper rod, were 9.45 mm for the 4340 ring, the 4620 ring, and the aluminum ring, whereas for the nickel and iron rings, the external radii were 9.68 mm. The inner radius, R_2, of the brass ring, which was the same for all trials, was 10.25 mm. Note that the slight difference in external and internal radii of the sample rings would cause only a change in their base capacitance, but would not affect the capacitance change values as measured by the bridge meter. The base capacitances were measured using the LCR meter for each case and were found to be 720 pF for the 4340 ring, 490 pF for the 4620 ring, 520 pF for the aluminum ring, 887 pF for the nickel ring, and 351 pF for the iron ring. The composition[23] of the 4340 steel ring is (with percent by weight) Ni 1.82, Cr 0.82, Mn 0.75, C 0.43, Mo 0.40, Si 0.33, Cu 0.07, V 0.069, Al 0.06, Co 0.014, Sn 0.007, P 0.066, Ti 0.003, S 0.001 and the balance is Fe. The composition for the 4620 steel ring is (with percent by weight) Ni 1.74, Mn 0.64, Al 0.28, Si 0.28, Mo 0.28, C 0.20, Cu 0.18, Cr 0.15, P 0.68, S 0.018, Sn 0.01, Co 0.01, As 0.005, V 0.002, Cb 0.002, Ti 0.001, Sb 0.001 and the balance is Fe. The other three rings, aluminum, nickel, and iron, are all of 99.99% purity and are elemental samples.

3-3. Capacitance Bridge Meter

The capacitance bridge meter was the most important component of our experiment in order to measure the magnetostriction effects. It is an old meter which has many possible control functions. This meter requires a 6V DC power supply in order to operate. This bridge meter is based on the principles of the Schering impedance bridge, with selectable combinations of inductors, capacitors, and resistors. There are four modes of operation, using the AC internal 1 KHz, AC external, DC internal 6 V, and DC

external. Out of these four possible functions we selected the AC internal 1KHz setting, because it is sufficiently larger than the frequency of variation of the capacitance in the sample ring, which was due to the 60 Hz applied current. For our internal power supply we used 6V DC (i.e., 4 D-cell batteries of 1.5 V each), which was very beneficial for reduced noise levels. This is because the DC supply more effectively isolates our data collection system from 60 Hz noise and its harmonics, which were present in our lab at high levels. Before using the capacitance bridge meter for our experiment we verified its capabilities and its degree of accuracy and precision for measurement by comparison to another meter for a standardized sample. For this purpose, a previous undergraduate student[24] used our machine shop to prepare a parallel plate capacitor which can be very minutely and accurately adjusted. The parallel plate capacitor is then calibrated with a handheld LCR meter so that a small change in the bridge meter from the null point in either direction will give a voltage signal that corresponds to known capacitance changes to the nearest 0.02 pF. To calculate the degree of the magnetostriction effect, the base capacitance was also needed for each sample, and it was measured before each experiment using the hand-held LCR meter. This value is then fitted with the value from the capacitance bridge meter by using the CGRL (balancing impedance) and DQ (bridge ratio) switch, with the meter after each trial being adjusted back to the same sensitivity setting for which it had been tested with the known capacitance changes. The adjustment of the bridge meter to the extremely sharp and narrow null point was the most challenging job, because of the extreme sensitivity of the capacitance bridge meter. With even a slight change in the Det Sens (sensitivity level) switch, the needle indicator of the null meter would sometimes move an almost unpredictably large amount. To obtain

reasonably clear magnetostriction data, the indicator in the scale display on the bridge meter must go to the null position. It was also noticed that the capacitor bridge meter worked better if it had sufficient warm-up time prior to the experiment.

3-4. Magnetic Field

As shown in Figure 3-2, the magnetic field at the point 'P' in the neighborhood of a long straight wire due to a small length 'dl' of a straight wire carrying a current 'I' given by Ampere's Law is

$$B = \frac{\mu_0 I}{4\pi} \int \frac{dl \sin\theta}{r^2} \tag{3-2}$$

where 'dl' is the small length of the wire and 'r' is the distance between the conductor and the point where the magnetic field is measured. It is convenient to carry out this integration in terms of the angle 'Φ', where 'Φ' is '$90^0 - \theta$'.

Therefore, $\text{Sin}\theta = \text{Cos}\Phi$

$$B = \frac{\mu_0 I}{4\pi} \int \frac{dl Cos\Phi}{r^2}$$

$$l = r_1 \tan\phi$$

Figure 3-2. (a) The magnetic flux density B at point P is calculated due to a current I flowing in a long straight wire.

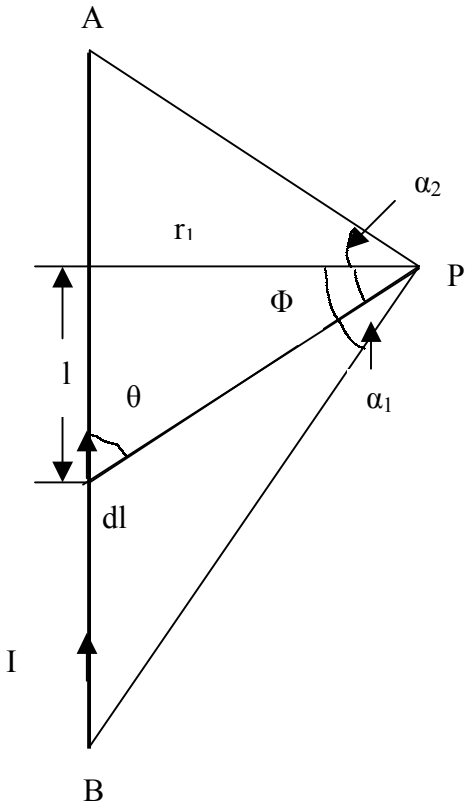

Figure 3-2. (b) Magnetic flux lines wrap circumferentially around the straight wire.

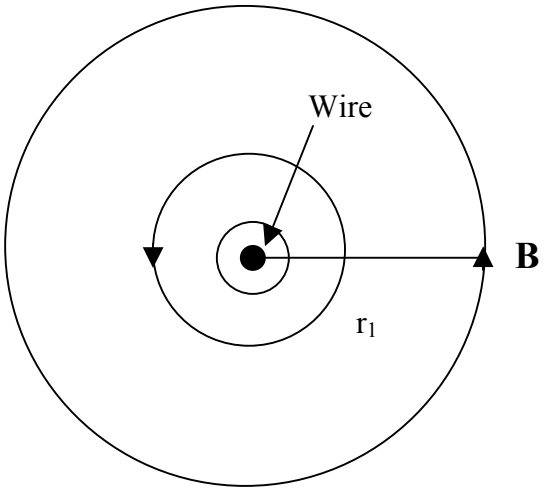

$$dl = \frac{r_1}{Cos^2\phi} d\phi$$

$$r = \frac{r_1}{Cos\phi}$$

$$B = \frac{\mu_0}{4\pi r_1} \int_{\alpha_1}^{\alpha_2} Cos\phi \, d\phi = \frac{\mu_0 I}{4\pi r_1} [Sin\phi]_{\alpha_1}^{\alpha_2}$$

Thus,

$$B = \frac{\mu_0 I}{4\pi r_1} (Sin\alpha_2 - Sin\alpha_1)$$

and B is perpendicular to r_1 and directed into the page, as given by the right hand rule. For a long conductor, $\alpha_2 = \pi / 2$ and $\alpha_1 = -\pi / 2$, thus

$$B = \frac{\mu_0 I}{2\pi r_1} \tag{3-3}$$

when the current, I, is passed through the welder rod, and the magnetic field, H, is generated along the circumference of the sample ring. Using equation (3-3), this field is given by:

$$H = \frac{\mu_0 I}{2\pi R_{1A}} \tag{3-4}$$

where R_{1A} is the zero-field outer radius of our sample ring. Substituting the value of the permeability of free space, μ_0, and current, I, from equation 3-1, we get

$$H = \frac{(4\pi \times 10^{-7}) \cdot (5 \times 10^{3} \cdot V_{drop})}{2\pi R_{1A}} [Tesla]$$

$$H = \frac{10 \cdot V_{drop}}{R_{1A}} [Oersted] \qquad (3\text{-}5)$$

where V_{drop} refers to the V(t) data from the shunt to the 'X-channel' of the storage CRO.

3-5. Storage CRO and Computer with LabView Program

The digital storage oscilloscope we used in this study can transmit and receive waveform data. It can transfer these waveform data in binary, hexadecimal, or ASCII encoding. For this study, an ASCII encoding waveform was used. This waveform is divided into a waveform preamble portion and waveform CURVE data (magnetostriction data). The waveform preamble contains the attributes for the associated waveform data. These attributes include the number of points per waveform, scale factor, vertical offsets, horizontal increment, scaling units, and data encoding. The preamble information is sent as an ASCII encoding string in all cases. The exact attributes sent depend on the waveform and the acquisition mode, and the setting used to obtain data. This storage CRO can respond with the preamble only, the curve data only, or the preamble and curve data together. Table 3-1 shows the commands for data transferring we used. The V(t) data from both the X and Y channels are transferred

Table 3-1. Commands to Transfer Data.

COMMAND	***FUNCTION***
sic	Send interface clear and set remote enable.
dat enc asc	Data encoding to ASCII
WFMpre?	Respond with preamble only
CURVe?	Respond with curve data only
WAVfrm?	Respond with the preamble and curve data together

together while the scope screen is saved in the XY mode.

LabView is a virtual instrument (VI) program, which utilizes the graphical programming language G. To receive the magnetostriction data from the storage CRO, our LabView program has 6 steps, which include GPIB board initialization, GPIB Write, and GPIB Read. Table 3-2 shows all virtual instruments (VI), which we used in our LabView Program, and Figure 3-3 and Figure 3-4 show the sequential graphic diagram for our LabView program.

Table 3-2. Virtual Instruments (VI) used in our LabView Program.

LabView Virtual Instruments	***Function***
GPIB write	Write data to the GPIB device identified by address string.
GPIB read	Read byte count (number of bytes) from the GPIB device at address string.
Write Characters to File.vi	Write a character string to a new byte stream file or appends the string to an existing file.
String Length	Returns the number of characters (bytes) in the input.
Select & Strip	Examines the beginning of string to see whether it matches true string, and returns a Boolean True or False depending on which string matched. Returns string with matched initial substring removed. If no match, output string is string.
SpreadSheet String to Array	Converts the spreadsheet string into an array of numbers or strings.
Reshape Array	Changes the dimension of an array according to the value of dimension size.
Decimate 1D Array	Divides input elements into output arrays, much like the way a decoder distributes the cards. Input must be 1D. Function is resizeable.
Build Array	Concatenate input in top to bottom order. Function is resizeable. Popup on an input and select change to array to change it to an array input.
Transpose 2D Array	Rearranges the elements of 2D array such that 2D array [i,j], where the 2D array can be any type.

Figure 3-3. The Sequential Diagram for our LabView Program

(From Step 0 to Step 2)

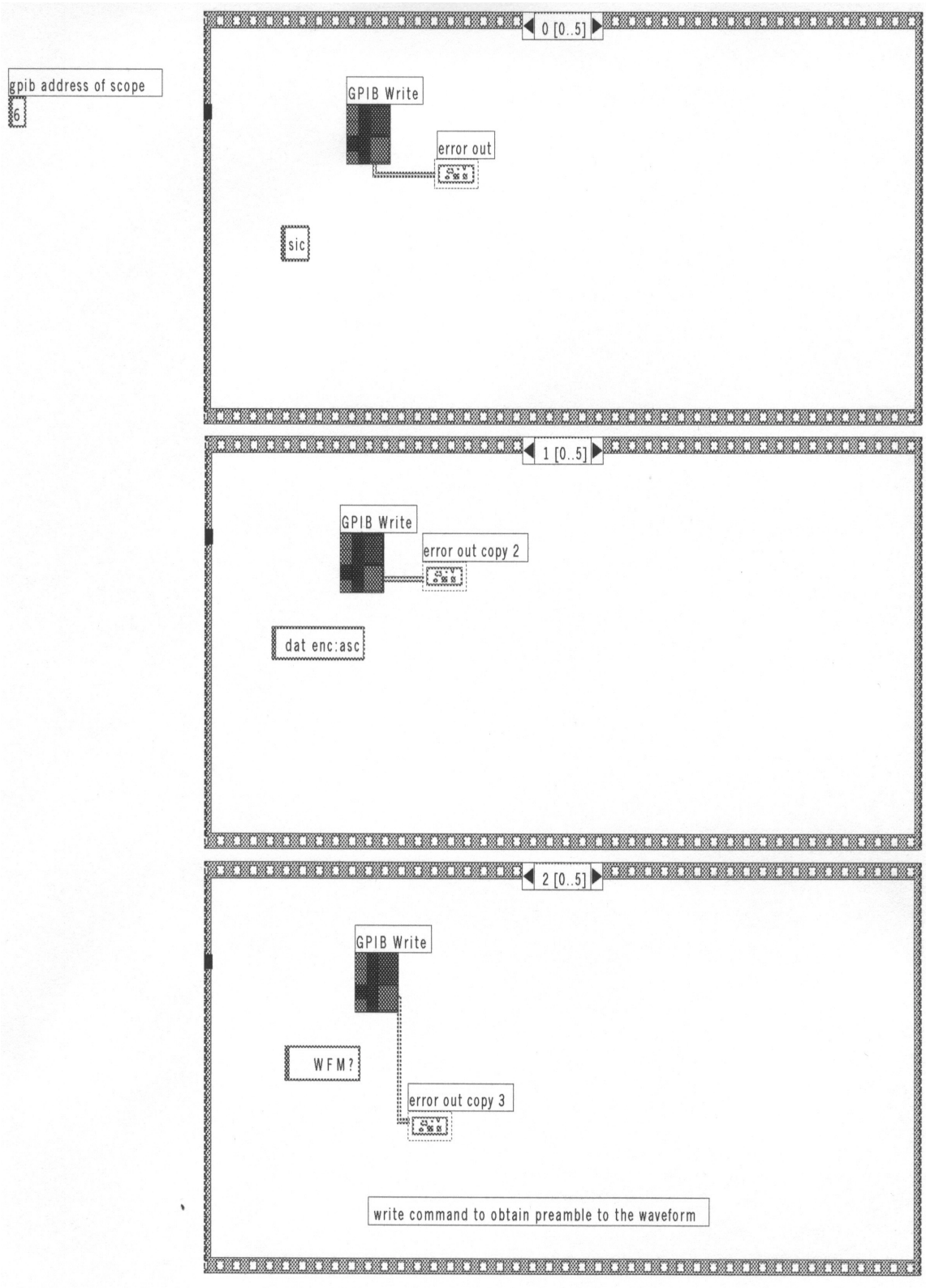

Figure 3-4. The Sequential Diagram for our LabView Program

(From Step 3 to Step 5)

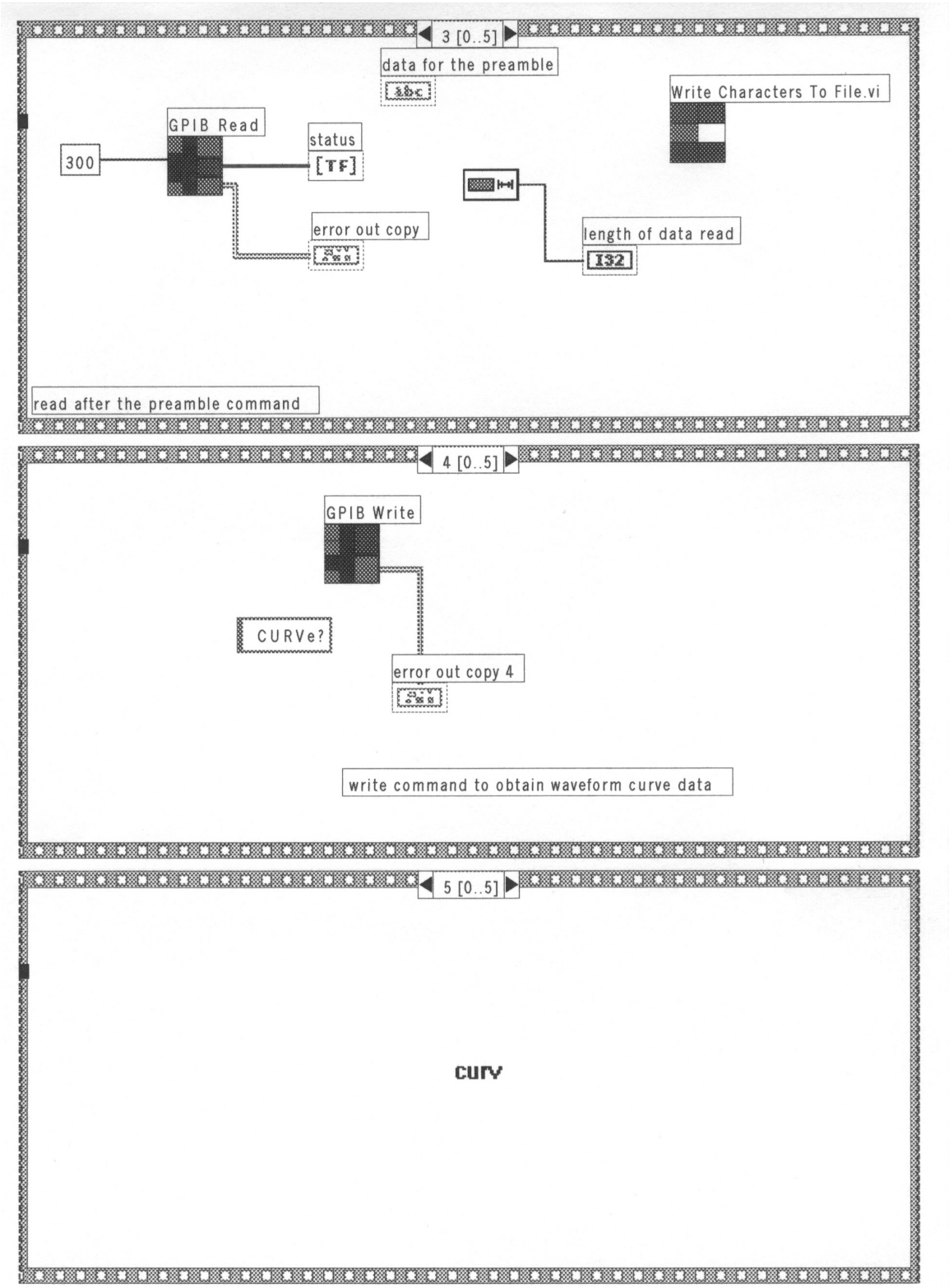

Chapter 4. Data Collection and Analysis

4-1 Raw Data and Time Data Generation

To plot the graph of magnetostriction ($\frac{\Delta l}{l}$) versus the applied magnetic field (H), we had to compare values of these quantities measured at simultaneous points in time. The time data was easily generated from our knowledge that the welder power supply produced 60 Hz AC current, so that the time elapsing during each period is given by

$$T = \frac{1}{f} = \frac{1}{60} = .0167\,\text{sec}$$

In this formula, T is the period of one cycle of the AC, and 'f' is the frequency of the supply current. Since there are 167 data points taken in each period, the sampling time, T_s, is given by, $T_s = 1/(60\times167) = 0.0001$ sec.

This is also expected, since the sampling frequency of the bridge meter is 10 points per oscillation cycle, and it operates on its own 1 KHz built-in AC frequency. Figure 4.1, Figure 4.2, Figure 4.3, Figure 4.4, and Figure 4.5 are the graphs plotted directly from the raw data that was dumped from the storage CRO to the computer. It can be seen that the input field is about the same for all of the graphs, because we used the same high current 60 Hz AC welder power supply to generate the applied field in each case. The output of the bridge meter is very different for the different samples, however. The nickel ring shows the largest oscillation whereas the iron shows the least oscillation. The oscillation absolute height is directly correlated to the magnitude of the magnetostriction. A large oscillation corresponds to a high level of magnetostriction. The control sample, the aluminum ring, does not display any oscillations that lie above the

Figure 4-1. The magnetostriction effect in the 4340 ring plotted from the raw data.

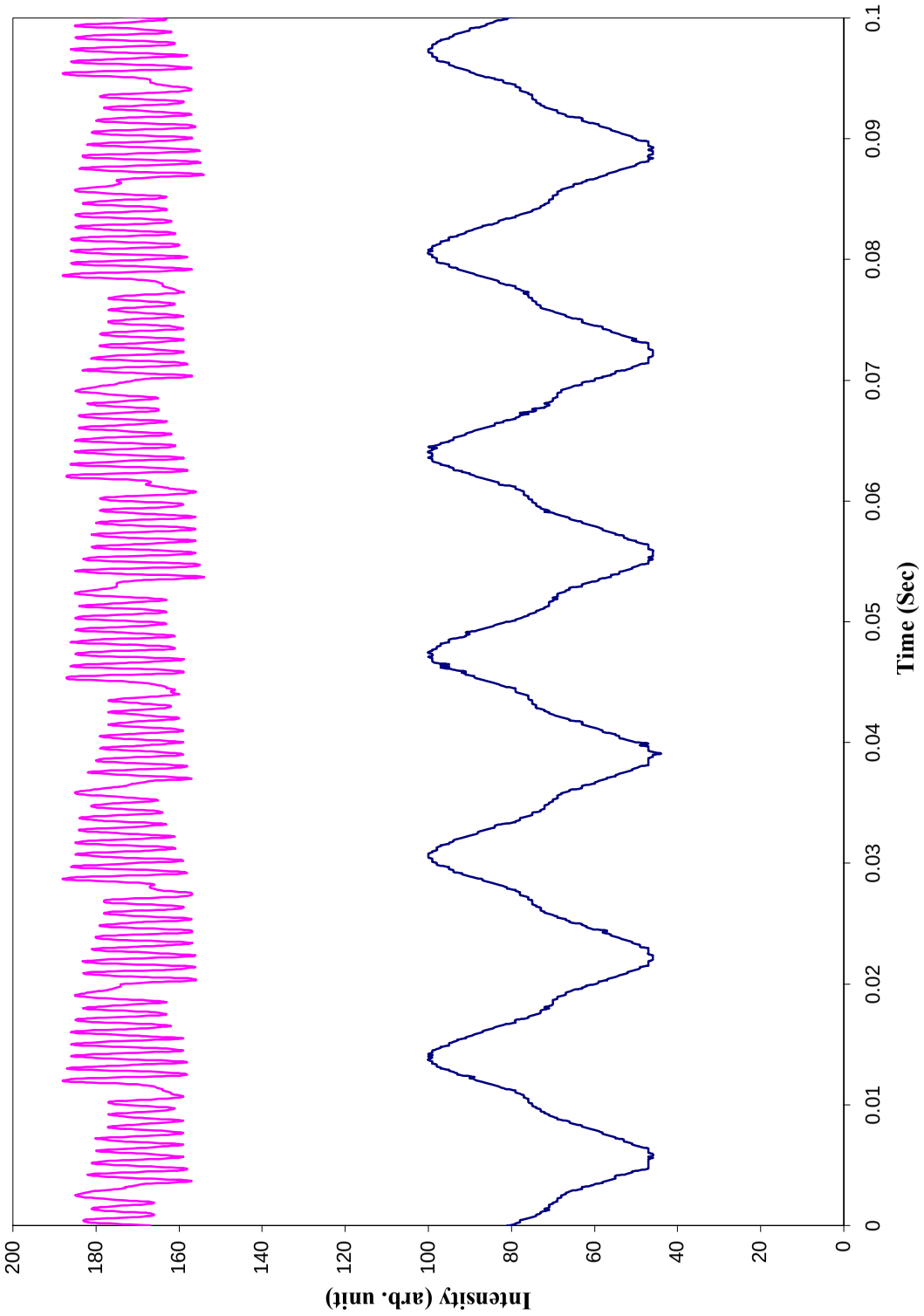

Figure 4-2. The magnetostriction effect in the 4620 ring plotted from the raw data.

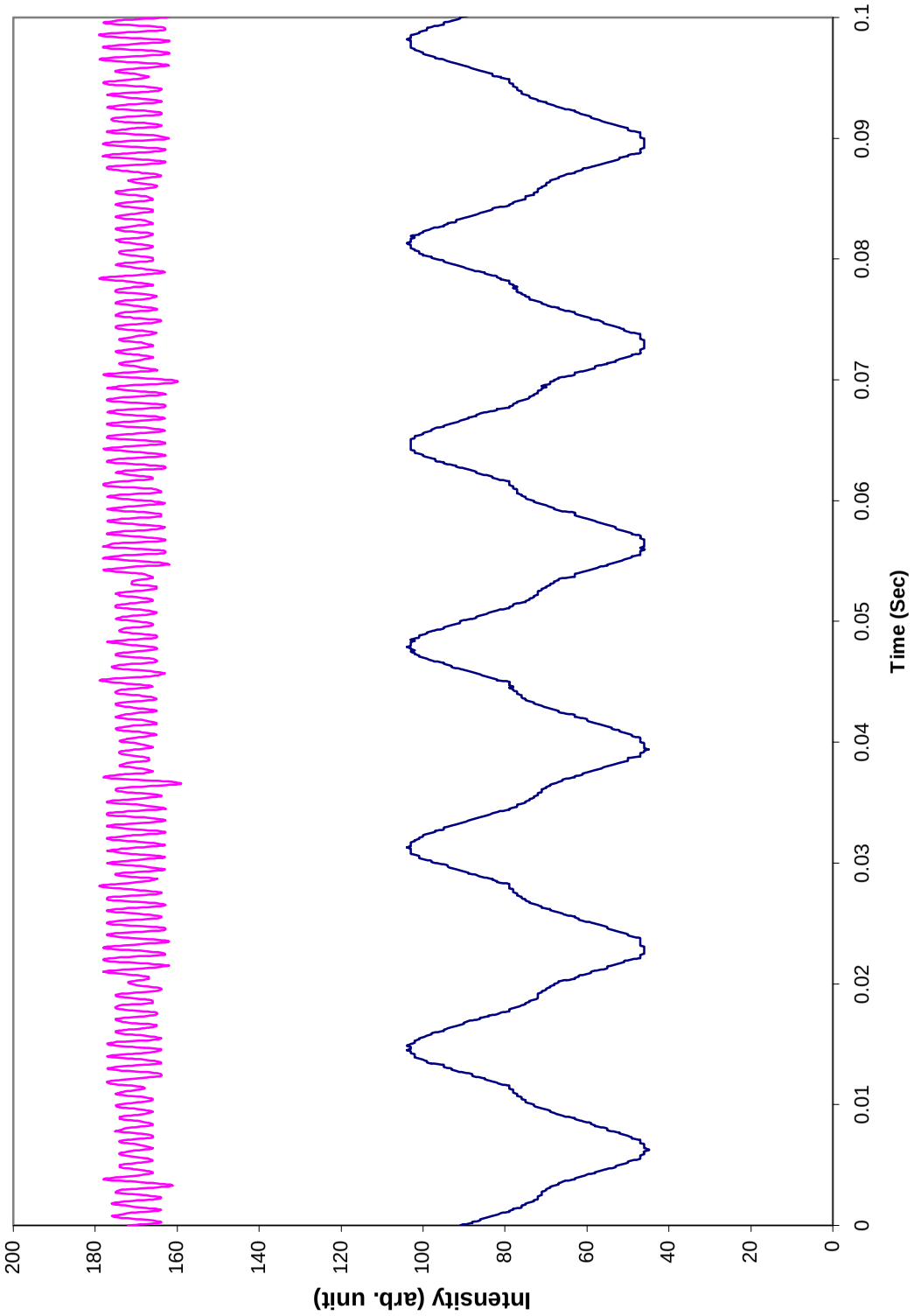

Figure 4-3. The magnetostriction effect in the nickel ring plotted from the raw data.

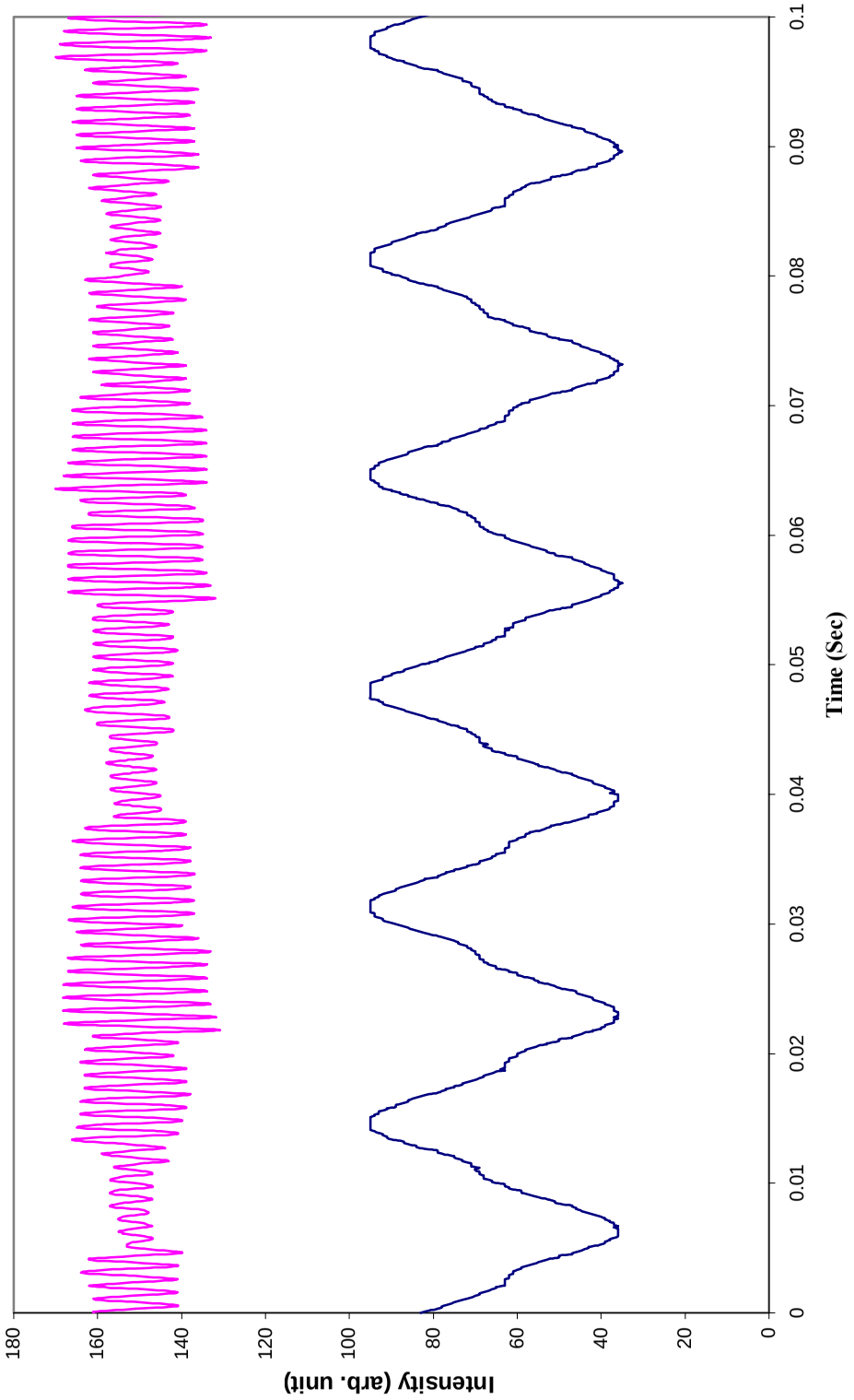

Figure 4-4. The magnetostriction effect in the iron ring plotted from the raw data.

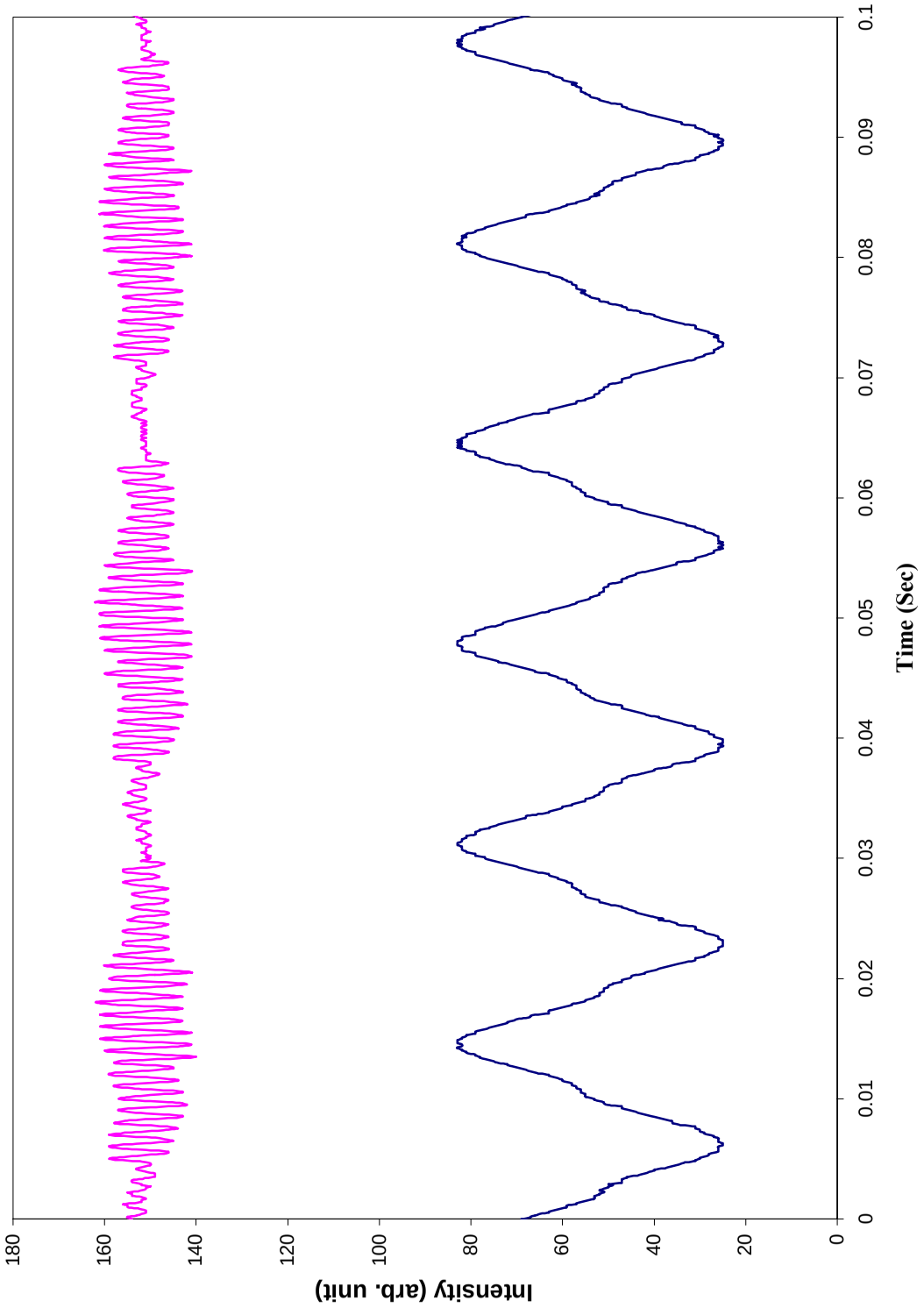

Figure 4-5. The magnetostriction effect in the aluminum ring plotted from the raw data.

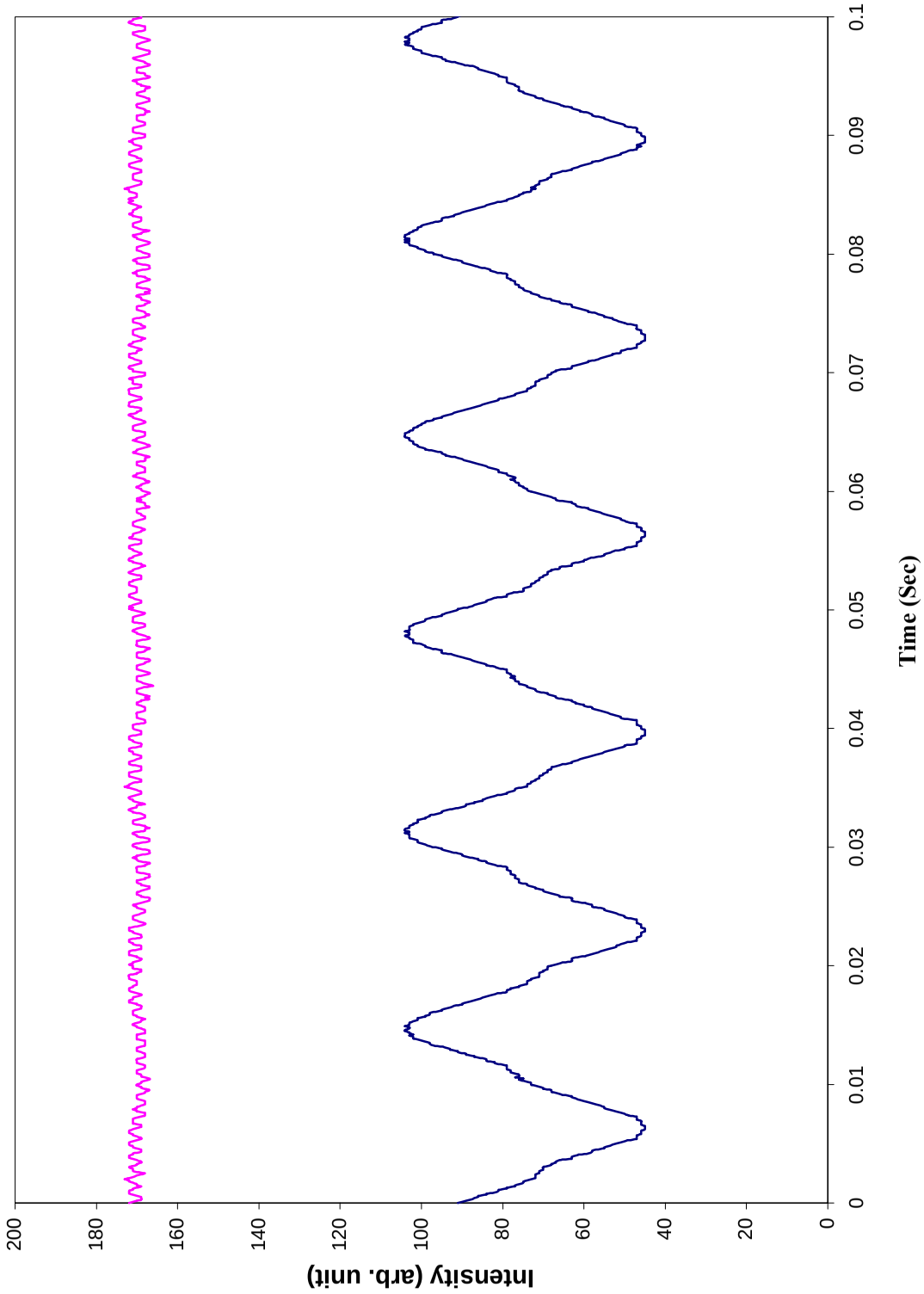

noise level, so it is obvious that it possesses no magnetostriction effect, as would be expected. The ideal waveform from the bridge meter output funneled through the storage CRO should approximately be enveloped by a sine wave, but it is more nearly enveloped by a square wave for the 4620 and the 4340 samples, whereas for the nickel and the iron it is almost the expected sine wave, but with varying amplitude (which is periodic). These variations of amplitude of the enveloping sine wave for our waveform are most likely due to a number of limitations in our laboratory, the prominent one being the presence of large 60 Hz noise levels and their harmonics. The square wave envelopes, however, are due to rapid saturation of the samples because of the large values of applied magnetic field in our experiments.

4.2 Generation of Butterfly Curve

The shape of the graph plotted between the magnetostriction ($\Delta l/l$) and the applied magnetic field (H) is generally characterized by referring to it as a "butterfly curve". To generate the butterfly curve from the raw data there are several crucial steps required. Table 4-1 is a sample raw data spreadsheet that has been collected from the storage CRO. The data from both channel X and channel Y have offsets as a result of the data transfer program that operates in a LabView environment. The offset values of X and Y were calculated for each ring using the values in the preamble file and then subtracted from the original data from the CRO. The offset values could also be clearly measured from the data as the average of the maximum and minimum values of the waveform data, both from the X and Y channels of the CRO. The offset value is subtracted from the raw data

Table 4-1. A sample Microsoft Excel spreadsheet of the raw data collected from the X and the Y channel of CRO is shown.

Time Data Seconds	Raw data V(t) Channel X	Raw data V(t) Channel Y
0	91	164
0.0001	90	166
0.0002	88	166
0.0003	88	169
0.0004	86	172
0.0005	86	175
0.0006	85	176
0.0007	84	174
0.0008	83	172
0.0009	82	168
0.001	81	165
0.0011	79	164
0.0012	79	166
0.0013	78	169
0.0014	78	172
0.0015	76	176
0.0016	76	176
0.0017	75	175
0.0018	75	172
0.0019	74	168
0.002	73	165
0.0021	73	165
0.0022	72	164
0.0023	72	166
0.0024	72	168
0.0025	71	171
0.0026	71	175
0.0027	71	175
0.0028	71	175
0.0029	71	174
0.003	70	171
0.0031	70	167
0.0032	69	163
0.0033	69	161
0.0034	68	162

from both the X and the Y channels, and then multiplied by the appropriate factor in the preamble file that was also transferred from the storage CRO. These factors differed according to the setting on the volts per division scale used for the X and the Y channels, respectively.

The applied magnetic field H(t) is then calculated by using the equation as given in Chapter 3 Section 5:

$$H(t) = \frac{10 \times V_{drop}}{r} Oe \qquad (4.1)$$

where V_{drop} is the channel X data from the CRO, and r is the radius of the sample ring when there is no magnetic field applied. But for the calculation of the magnetostriction ($\Delta l/l$) we used the equation from Chapter 2 Section 8:

$$\frac{\Delta l}{l} = \frac{\exp[\ln R_2 - \frac{C}{C + \Delta C}(\ln R_2 - \ln R_1)] - R_1}{R_1} \qquad (4.2)$$

where R_2, R_1, C, and ΔC are the radius of the outer ring, the radius of the inner ring, the base capacitance, and the change in capacitance as measured by the bridge meter, respectively. The bridge meter has an output voltage signal which is proportional to ΔC, the capacitance change from the base value after the meter has been nulled. This output voltage has to be calibrated against a known capacitance change prior to the actual experiment to get the transfer value from bridge output voltage to capacitance change. To measure the change in capacitance, a sine curve is fitted on the raw data after subtracting the offset value from the channel Y data of the CRO.

To fit the best curve, the average of the maximum and minimum values of the data from channel Y was taken into consideration. The curve was best fitted in a manner

to most nearly envelope all the oscillating waves from channel Y of the CRO into a sine wave. The corresponding points of the fitted sine wave as a function of time give a voltage which is proportional to the value of the change of capacitance. The curve fitted sine wave, after subtracting the offset value for all of the sample rings, is shown in Figures 4-6 through 4-9. After calculating both the magnetic field H(t) and the magnetostriction ($\Delta l/l$) within this Microsoft Excel spreadsheet, $\Delta l/l$ is plotted against H(t) using the Microsoft Excel program. Table 4-2 shows a sample of the data analysis as contained in the Microsoft Excel spreadsheet. In these figures it can be seen that the maximum magnetostriction effect was observed in the nickel ring, as expected, and that it is nearly half of the value of magnetostriction as would be expected from Bozorth[25], as predicted for the single ring of our experiment, and as mentioned in chapter 3.

The "butterfly-shaped" curve, as shown in Figures 4-10 to 4-13 for our different sample materials, is due to the small phase difference, or domain hysteresis, between the magnetostriction ($\Delta l/l$), and the applied magnetic field H(t). This can also be thought of as the recovery time of a domain to the random orientation, i.e. a phase lag, as also tabulated in Table 4-3. If there were no phase difference, then the shape would be like a 'V' curve as shown in Figure 4-14 (a). The "butterfly shape" is generated whenever the samples possess a lagging rotation of the domains, as shown in the ideal development stage in Figure 4-14 (b).

The magnetostriction values measured in our experiments are tabulated in Table 4.3. They are nearly the same for the steel samples as observed by Magnalastic Devices, Incorporated (MDI), a subsidiary of Methode Electronics, via private communication of

Figure 4-6. Sine curve fitting in the 4340 ring.

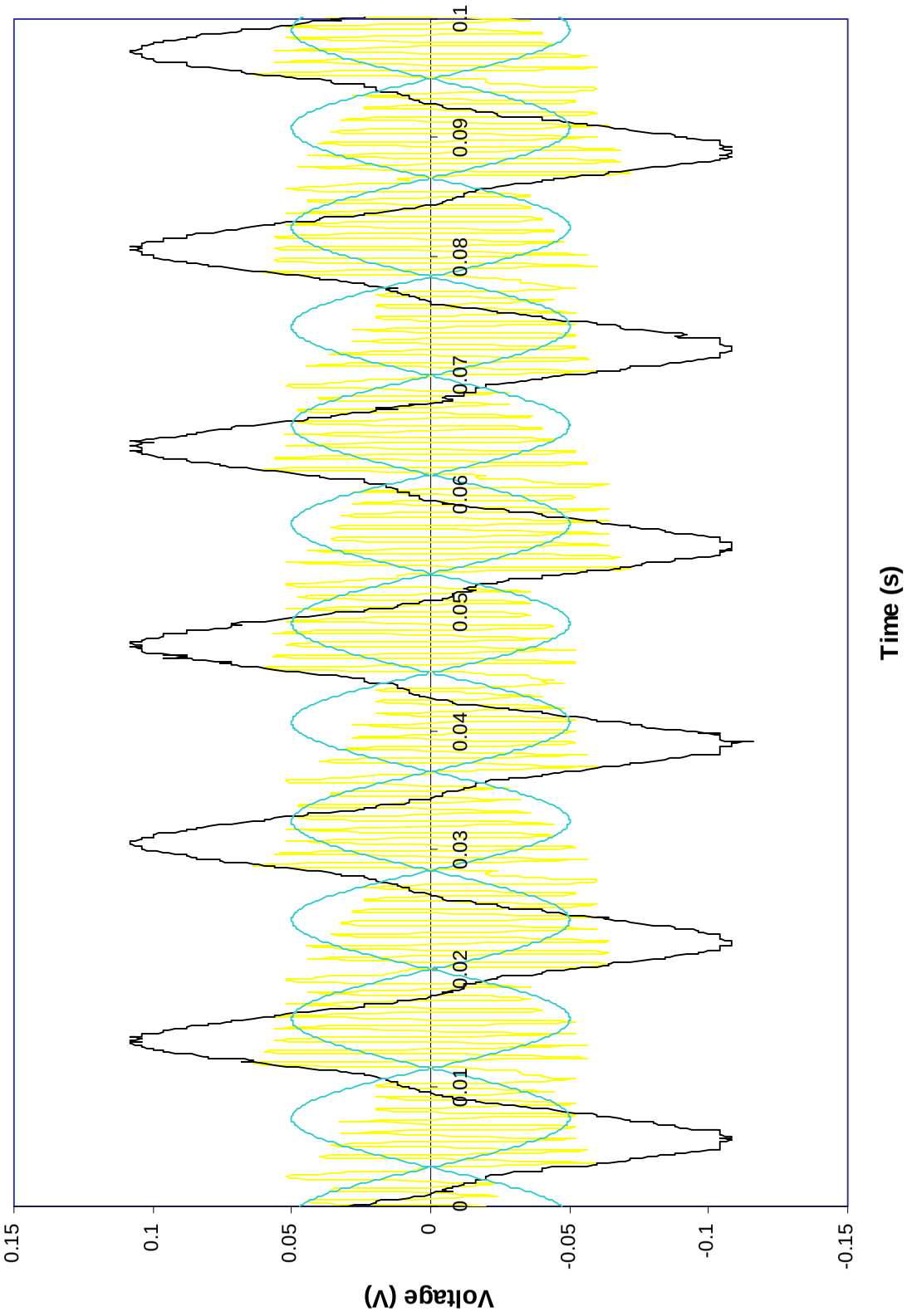

Figure 4-7. Sine curve fitting in the 4620 ring.

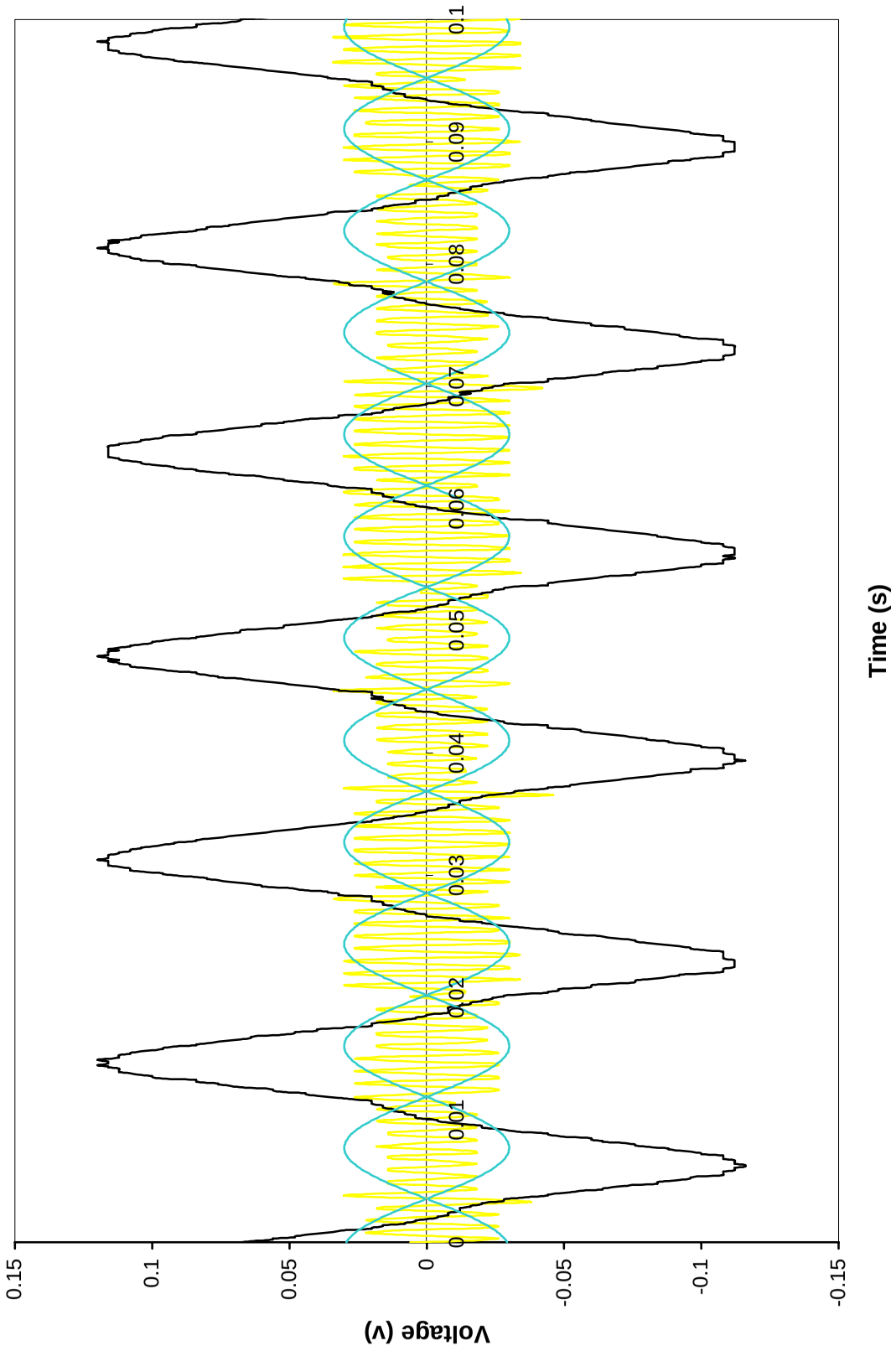

Figure 4-8. Sine curve fitting in the nickel ring.

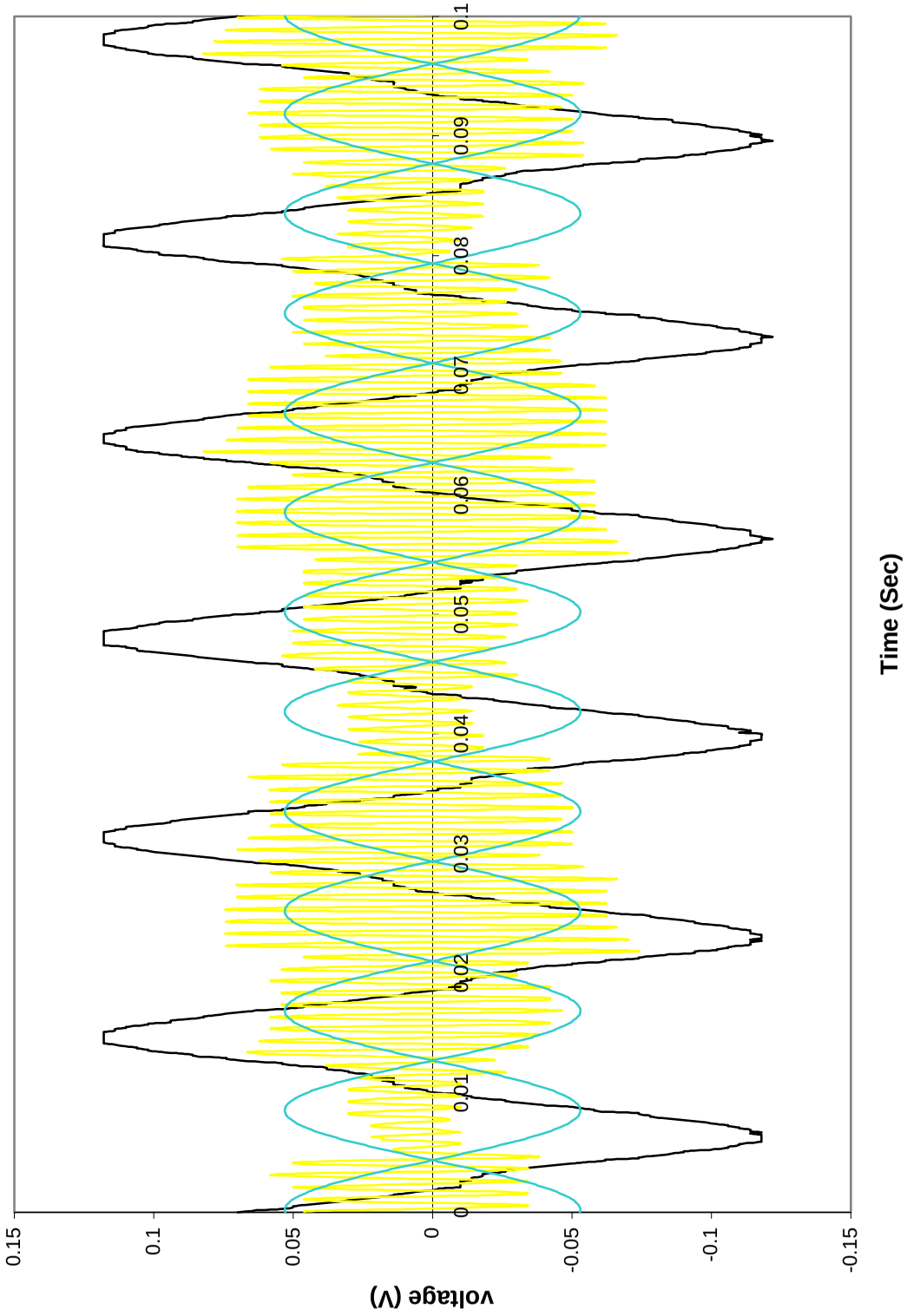

Figure 4-9. Sine curve fitting in the iron ring.

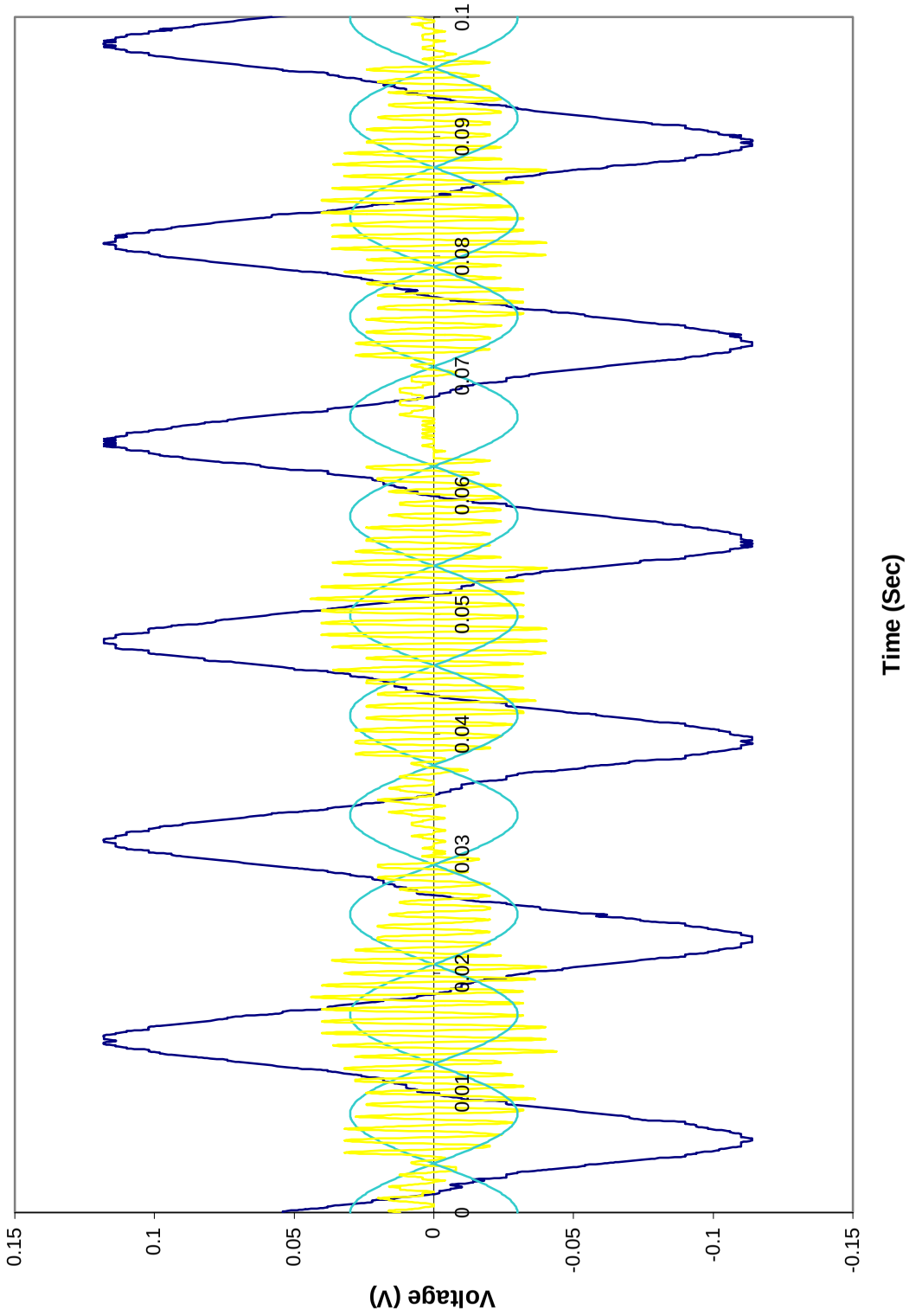

Table 4-2. A sample Microsoft Excel worksheet used to generate the butterfly curve is shown.

Magnetostriction Measurement Template for Nickel

Base Capacitance(pF):	887
Inner Diameter of Ring Holder (m):	0.0205
Outer Diameter of Sample Ring (m):	0.019365

TIME (Sec)	CURRENT (Shunt V)	CHA CAP (Volts)	INVERT CAP CNG	CURRENT (Amps)	H FIELD (Oe)	CAP CNG PF	DEL/L (ppm)
0	0.046	0.0001	0.0528	350	72.61	0.1252	0.04187
0.0001	0.046	0.066	0.05297	350	65.46	0.1255	0.00107
0.0002	0.03	0.002	0.053	310	64.46	0.1254	0.01285
0.0003	0.006	0.054	0.0528	270	64.51	0.1251	0.06565
0.0004	-0.014	0.05	0.05223	250	56.01	0.1247	0.57
0.0005	-0.034	0.05	0.05159	250	51.86	0.1247	0.13
0.0006	-0.034	0.05	0.0499	250	51.86	0.1235	0.251
0.0007	-0.022	0.016	0.047	230	47.71	0.12226	0.394
0.0008	-0.002	0.042	0.049	210	43.58	0.121	0.56
0.0009	0.026	0.038	0.0456	198	39.41	0.11975	0.773
0.001	0.042	0.034	0.0466	170	35.26	0.1182	1.007
0.0011	0.038	0.03	0.045	150	31.12	0.1165	1.5665
0.0012	0.034	0.026	0.5435	130	26.97	0.1147	11.887
0.0013	0.03	0.022	0.023	110	22.82	0.1127	2.238
0.0014	0.026	0.018	0.0411	90	18.67	0.1105	2.617
0.0015	0.022	0.014	0.0398	70	14.52	0.1087	3.023
0.0016	0.018	0.014	0.039	70	14.52	0.1057	3.023
0.0017	0.014	0.051	0.038	50	10.37	0.103	3.456
0.0018	0.01	0.006	0.037	30	6.22	0.1003	4.4
0.0019	0.0012	0.002	0.035	10	2.07	0.09779	4.652

Figure 4-10. The butterfly curve for the iron ring, where the graph is the magnetostriction in ppm vs. the applied magnetic field in oersteds.

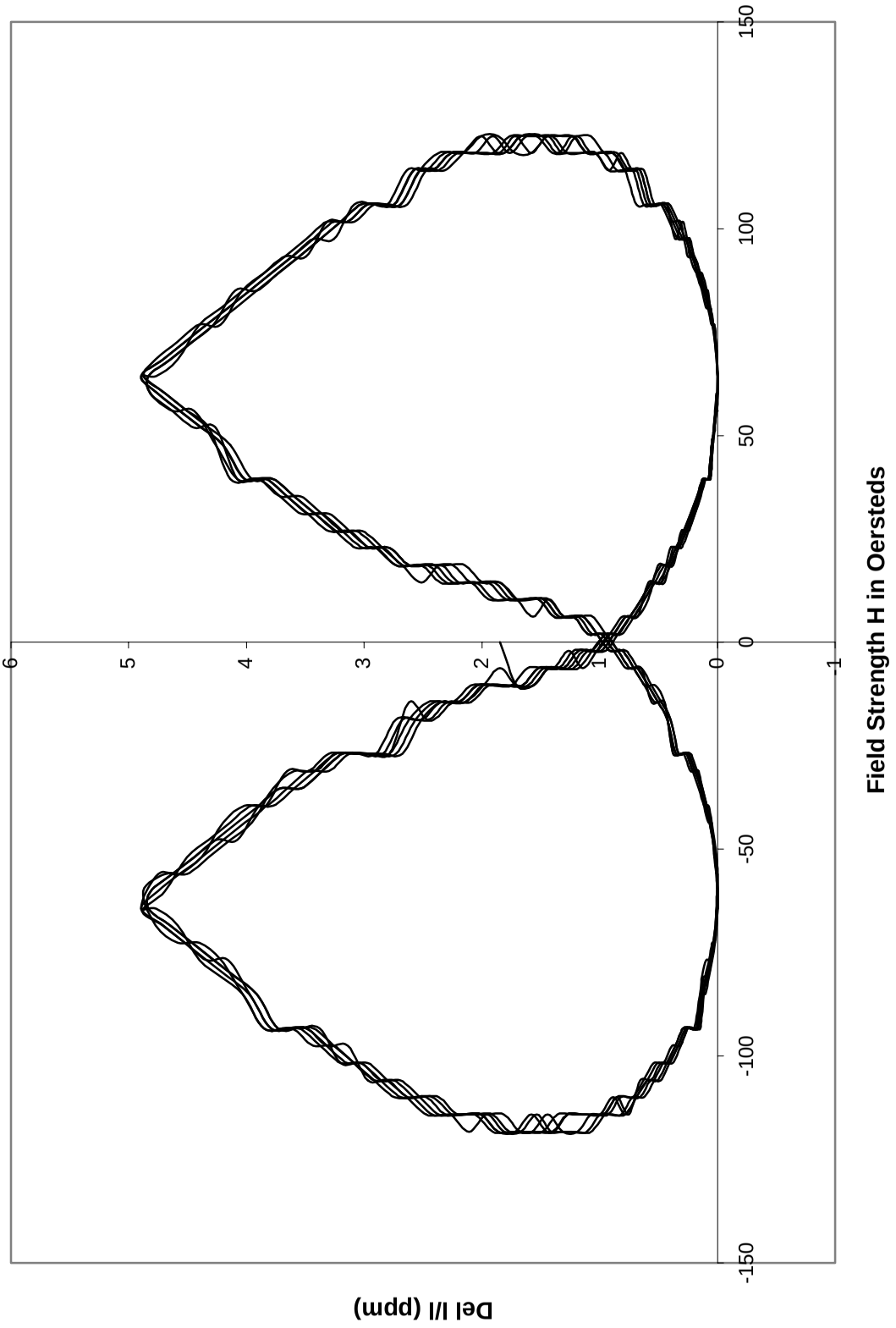

Figure 4-11. The butterfly curve for the nickel ring, where the graph is the magnetostriction in ppm vs. the applied magnetic field in oersteds.

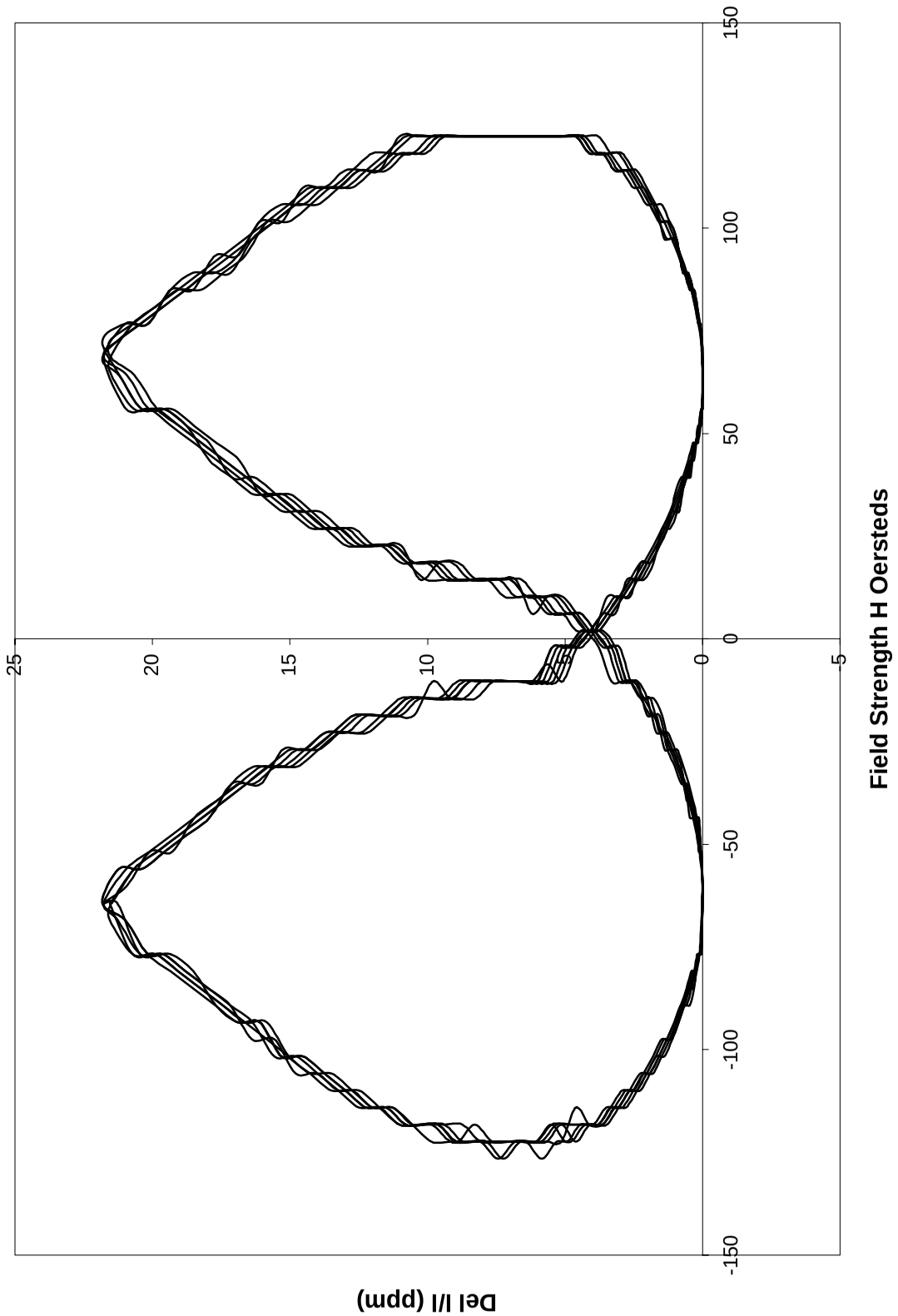

Figure 4-12. The butterfly curve for the 4620 ring,where the graph plotted is the magnetostriction in ppm vs. the applied magnetic field in oersteds.

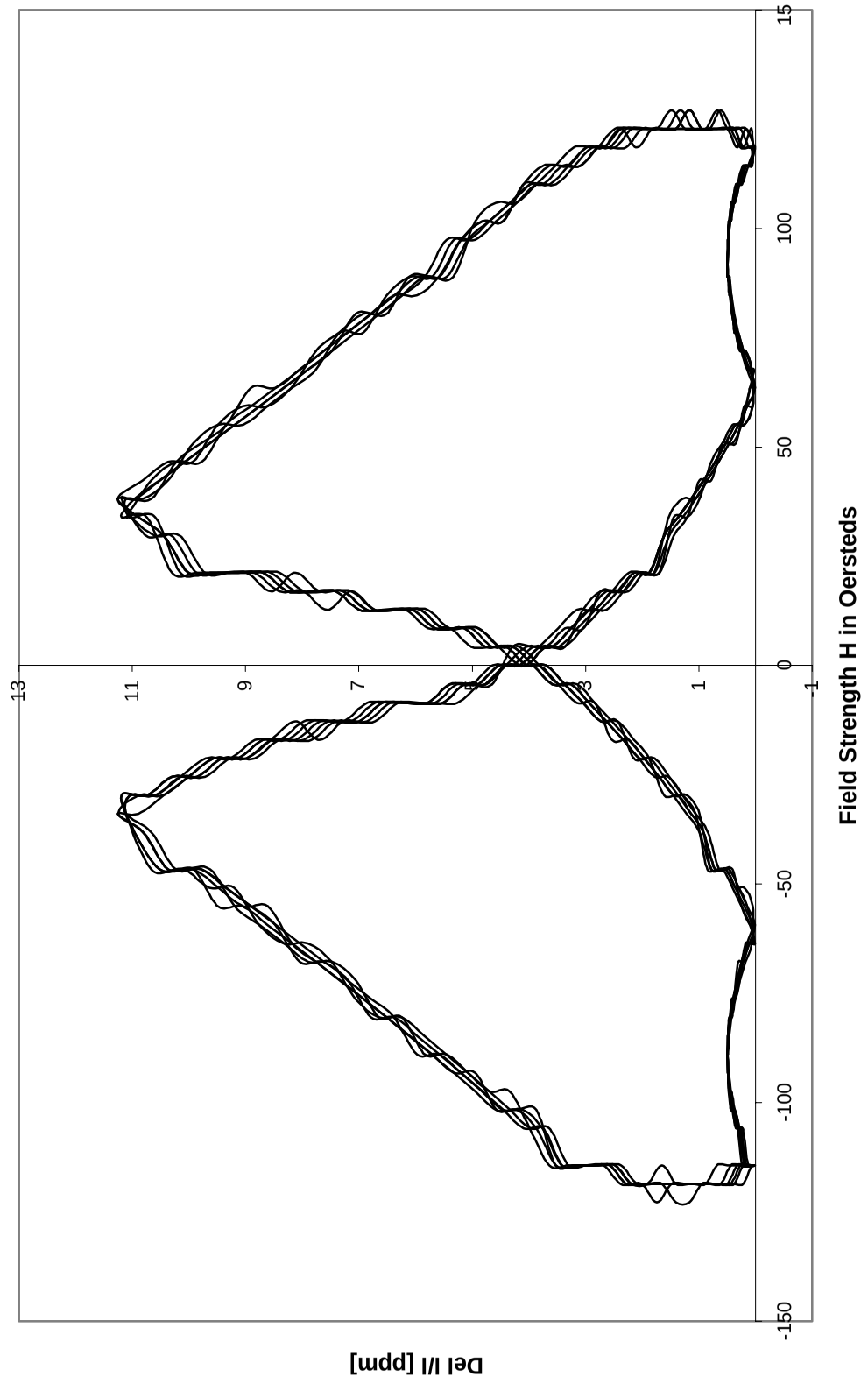

Figure 4-13. The butterfly curve for the 4340 ring, where the graph plotted is the magnetostriction in ppm vs. the applied magnetic field in oersteds.

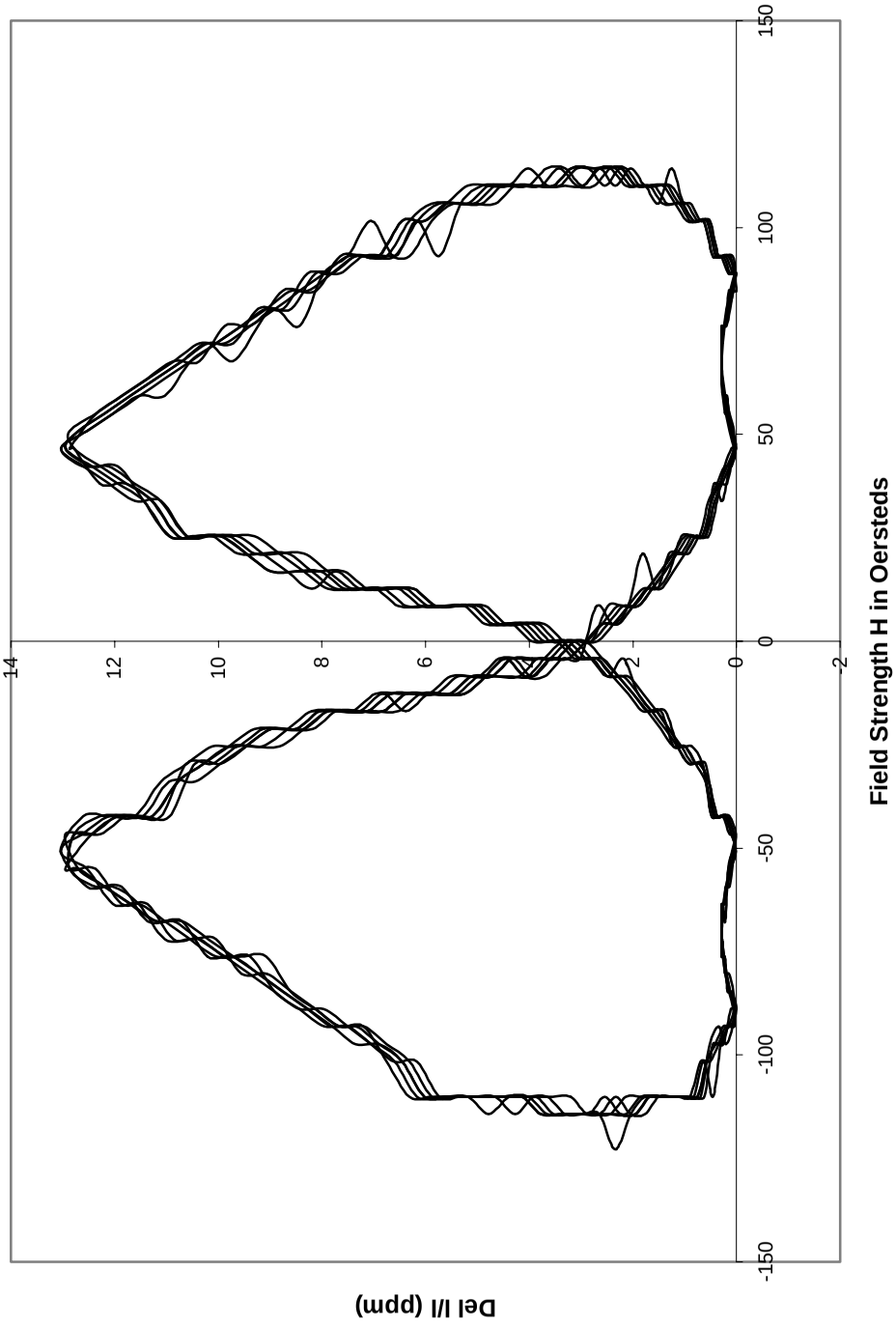

Table 4-3. The tabulated values* of measurement of the magnetostriction are shown.

Sample Materials (Ring)	**Observed Magnetostriction** (ppm)	**Maximum Field Strength** H (Oe)	**Expected Magnetostriction** (ppm)	**Recovery Time** (ms)
Nickel	22	122	35 to 40	1.1
Iron	5	122	7 to 8	2.7
Steel (4620)	11	127	15 to 20	1.8
Steel (4340)	13	114	20 to 25	1.7

* The magnetostriction values in the table are the single highest value observed in each case from the butterfly curve at the highest value of applied magnetic field. The data can be compared with Figures 4-15 and 4-16, in which each point of these graphs could be associated with a butterfly curve of its own. It is clear that our values for the iron and nickel in the table would lie on or near the curves in these Figures, and approach the saturation values of magnetostriction.

Figure 4-14. (a) Ideal curve, magnetostriction in ppm vs. applied magnetic field in Oersteds, when there is no phase difference, or lagging of domain rotation.

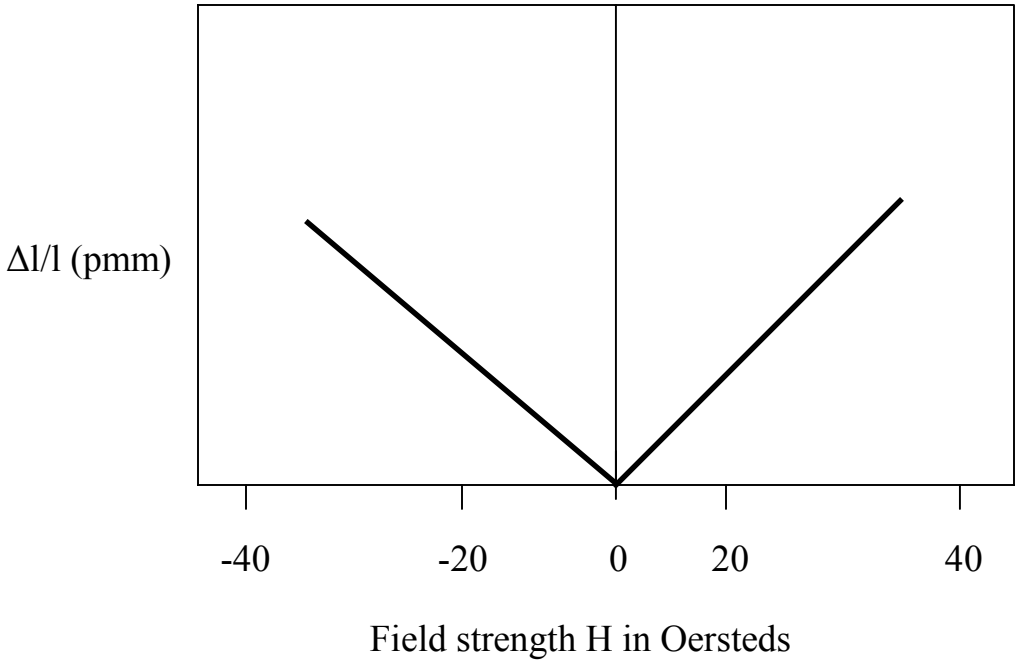

(b) Graph, magnetostriction in ppm vs. applied magnetic field in Oersteds, when there is phase difference, or lagging of domain rotation.

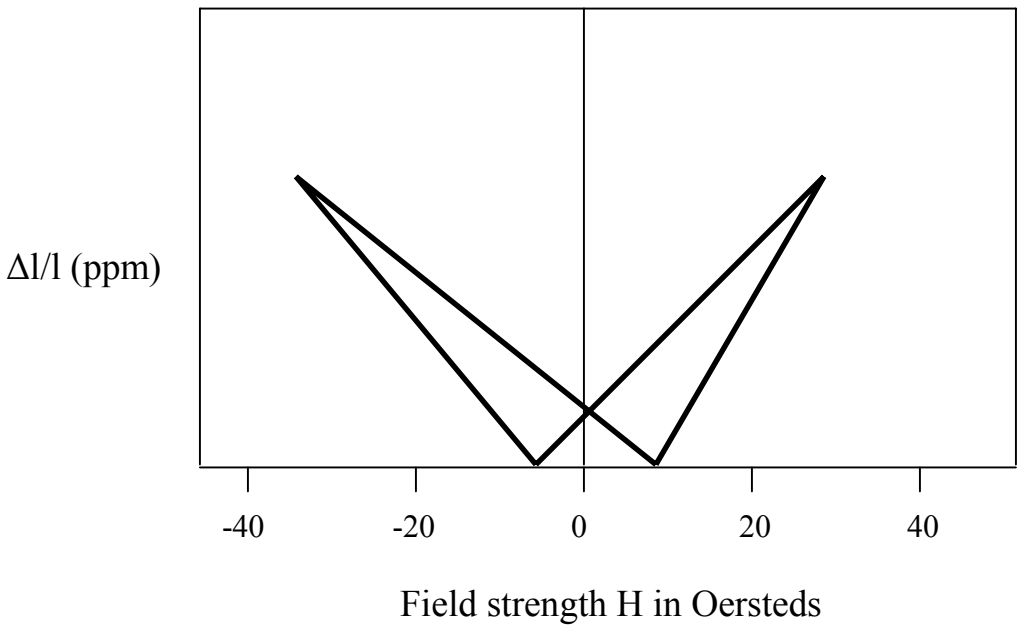

unpublished data. The values obtained for nickel and iron, as explained in Table 4-3, are nearly the same as published data, as shown in Figure 4-16[26].

4-3 Comparison with Previous Results

After analysis of our data the magnetostriction levels of all four samples can be easily observed and compared from the "butterfly" graphs. It is found that the nickel ring demonstrates the maximum magnetostriction, followed by the 4340 steel, the 4620 steel, and finally by iron, respectively, in decreasing order. In Figures 4-15 and 4-16 the magnetostriction is plotted against the magnetic field strength for four magnetic materials[27], iron, nickel, cobalt, and permalloy, from earlier literature[28]. The magnetostriction, $\frac{\Delta l}{l}$, is measured in the same direction as that of the applied magnetic field, H, in all of these cases. It can be clearly seen from Figure 4-15 that in the weak field, both iron and permalloy expand, and both cobalt and nickel contract. On the other hand, in the high magnetic field, it can be seen from Figure 4-16 that iron will later contract and that all curves only begin tangent to the H-axis. Then in the strong field they approach limiting values, so that there is only a small length change with the application of additional field strength that is known as the volume effect, as shown in Figure 4-16. The magnetostriction of three materials against the intensity of magnetization is plotted at low field strengths in Figure 4-17. It can be seen that very little change in length occurs before the magnetization rises to the steepest part of the magnetization curve, by comparing this figure with the curves in Figure 4-15. This is because most of the magnetostriction occurs during the large-scale rotation of the domains. This is the reason why the increase of magnetostriction at field values approaching remanence is quite

Figure 4-15. Magnetostriction of some common materials showing expansion or contraction. The figure is reprinted from Bozorth (1968).

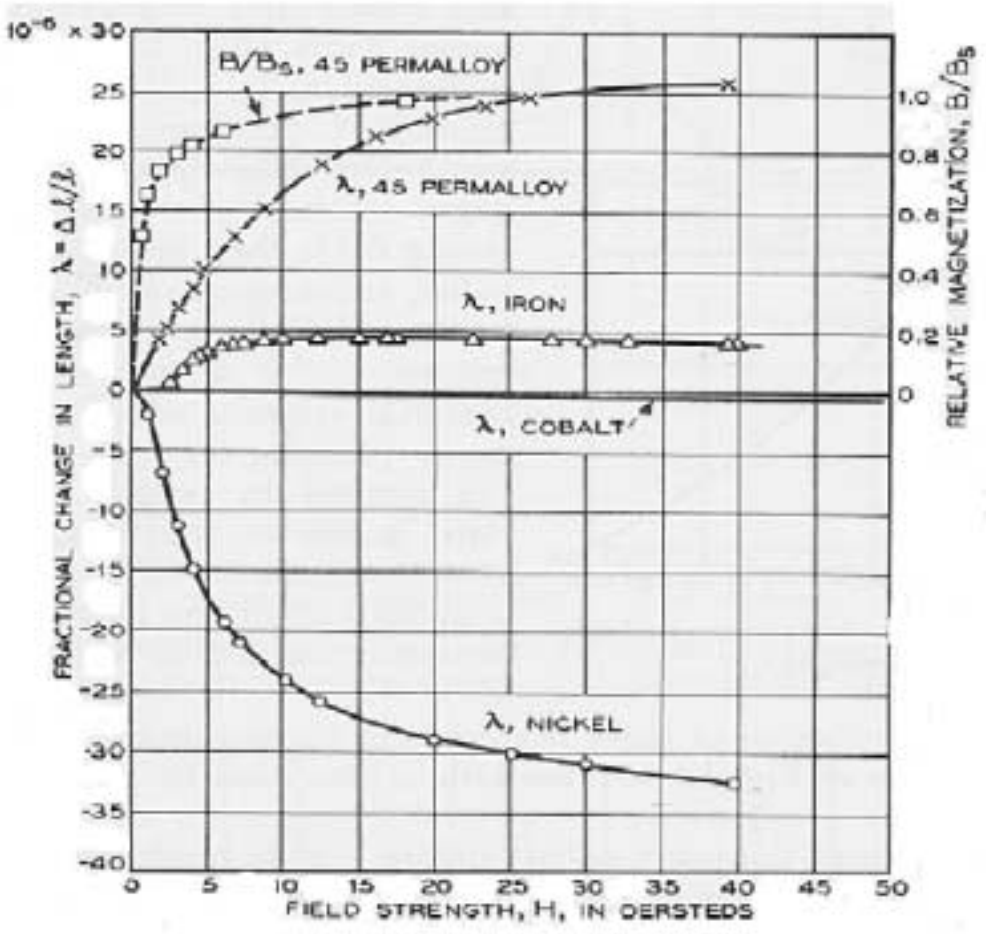

Figure 4-16. Magnetostriction at high field strengths. The figure is reprinted from Bozorth (1968).

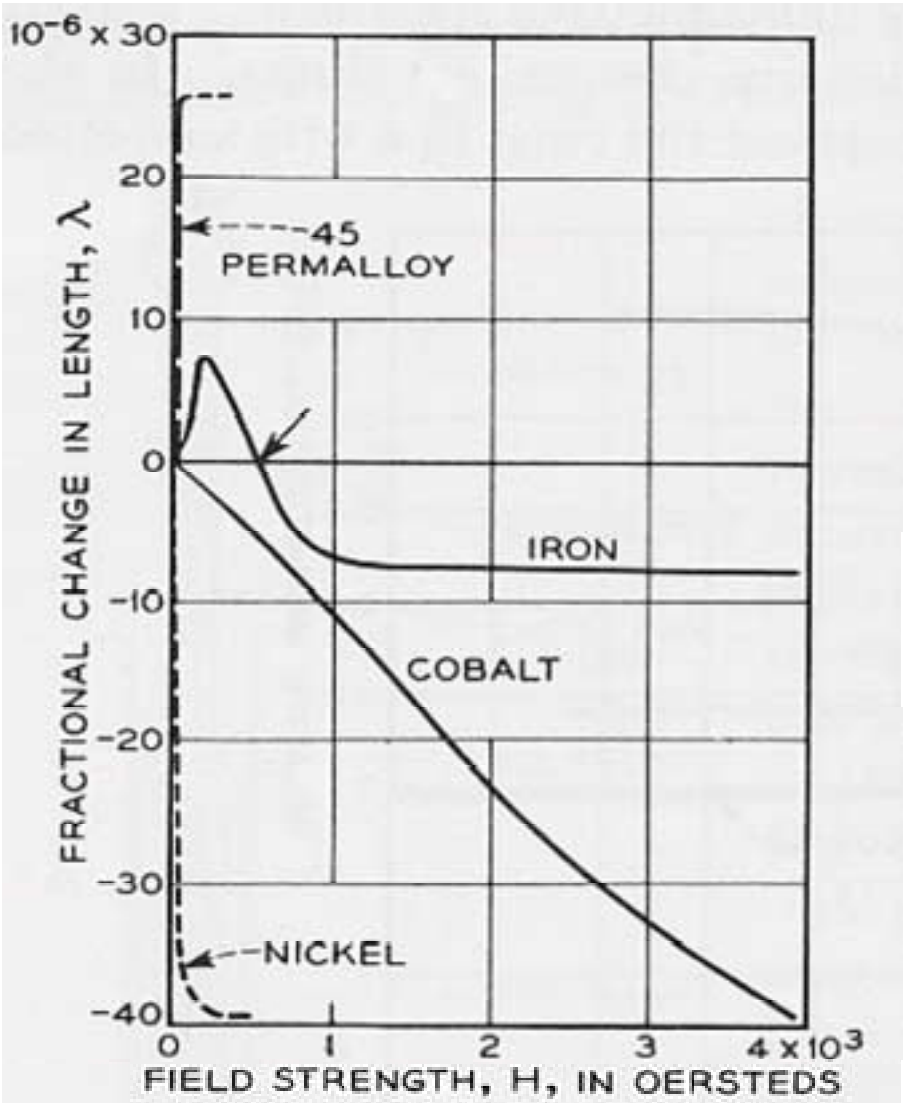

Figure 4-17. Magnetostriction as dependent on the intensity of magnetization at low field strengths. Figure is reprinted from Bozorth (1968).

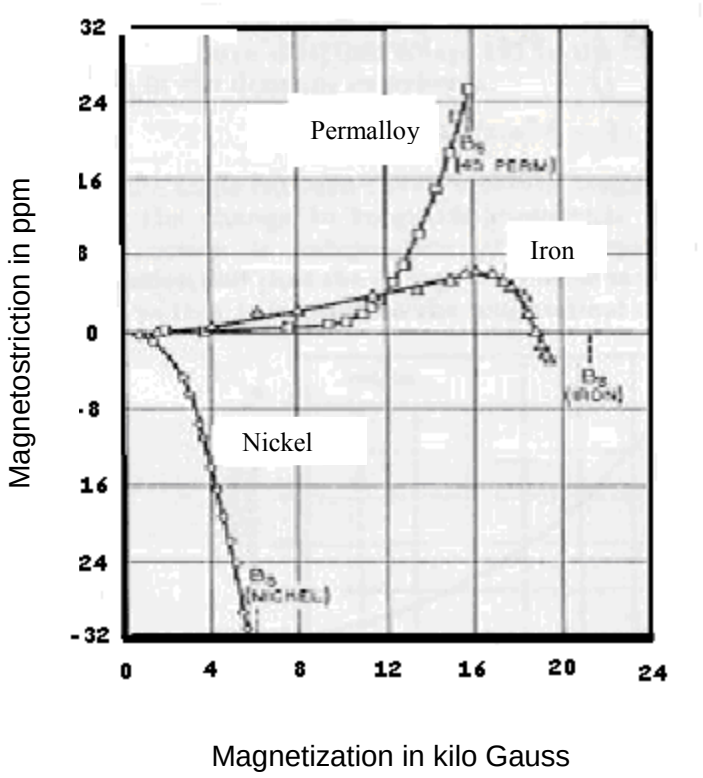

small, as can be seen in the tails on either side of the hysteresis curve for the magnetostriction of iron, as shown in Figure 4-18. This correlation between the magnetization and magnetostriction curves of a ferromagnetic materials can also be seen by comparing Figure 1-8 with Figure 1-2. The increase in magnetostriction is large only in the steepest part of the curve before saturation is reached. When the magnetization approaches saturation, the magnetostriction also approaches its limiting value, which is known as saturation magnetostriction.

Nickel

Nickel has the maximum contraction in the applied magnetic field as compared to other materials, which has already been shown in Figure 4-15. The magnetostriction in nickel is from 25 to 47 ppm depending on the composition, the heat treatment, and the methods of measurement and extrapolation. The best value of magnetostriction in nickel is taken to be 34 ppm[29]. In weak fields the curve is characteristically flat, and when the magnetic field is half the value of the saturation, H_s, the magnetostriction[30] is only one fifth of the saturation value, $(\frac{\Delta l}{l})_s$ as can be seen in Figure 4-19 for the case of 100% nickel in iron, which would occur at the extreme right-hand side of the figure. A hysteresis loop for a well annealed specimen[31] and loops for hard drawn (H_c=27Oe) and partially annealed specimens (690^0 C, H_c= 4.7Oe) are shown in Figure 4-20. Both the transverse expansion by Fricke[32], in low as well as in high fields, and Masiyama's result, are shown together in Figure 4-21.

Figure 4-18. The hysteresis of magnetostriction in iron, which shows the magnetostriction change at remanence is low, as evidenced by the tails of the curve. The figure is reprinted from Bozorth (1928).

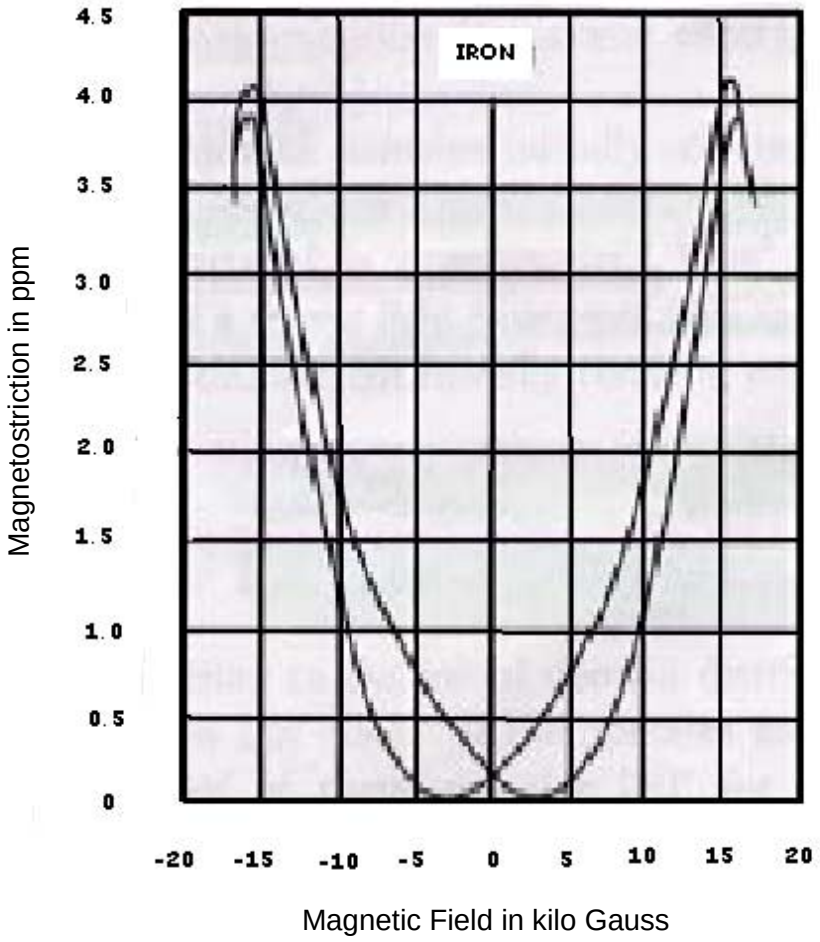

Figure 4-19. The magnetostriction of iron-nickel alloys at various fractions of saturation. The figure is reprinted from Bozorth (1928).

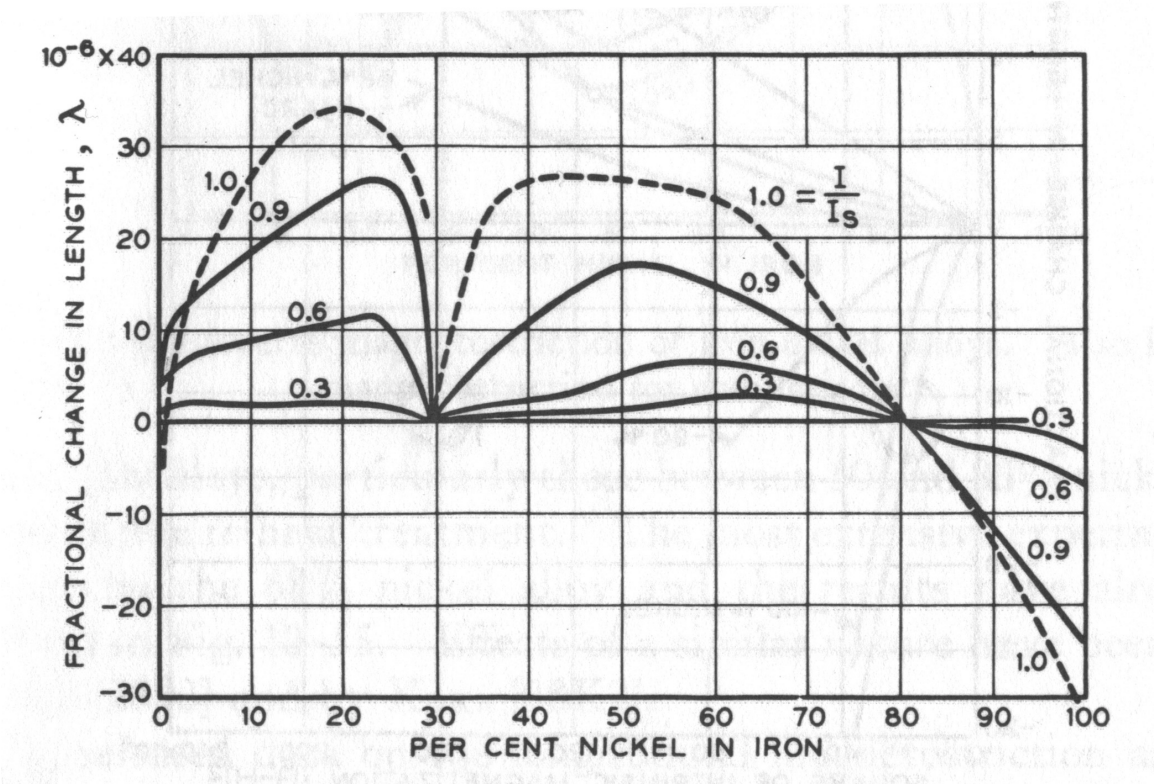

Figure 4 -20. Hysteresis of magnetostriction in nickel in various conditions is shown.

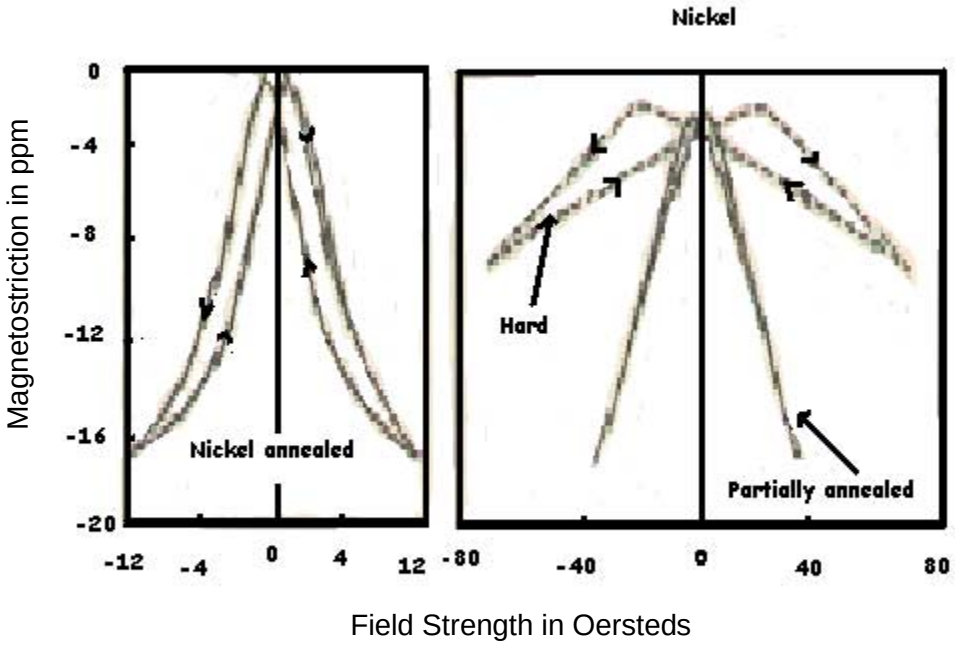

Figure 4-21. The magnetostriction of nickel, according to Fricke and Masiyama. The figure is reprinted from Bozorth (1931).

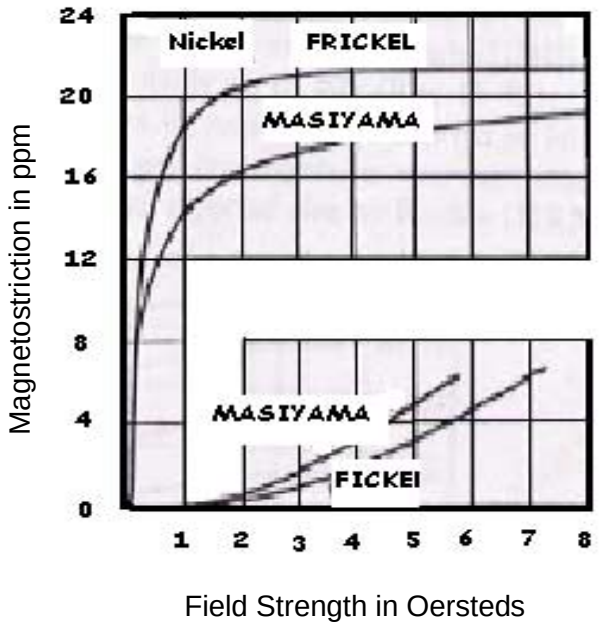

Iron

Figure 4-15 shows how the magnetostriction of iron increases with increasing field strength. In the different values of applied magnetic field, Figure 4-22 shows how the length increases until it reaches the maximum and then decreases to its original length around 200 and 300 Oersteds, and then continues to decrease in length as the field strength increases. Purity, heat treatment, and the dimensional ratio of the specimen will slightly affect the shape of the curve, but in general its character remains the same. The hysteresis loop of Figure 4-23 in which magnetostriction is plotted against the magnetic field, H, is compared with Figure 4-18, which shows $\frac{\Delta l}{l}$ versus magnetic field, according to Masiyama.

Iron – Cobalt Alloys

Early experiments on the measurement of these alloys were made by Honda and Kido[33] and then followed by Schulze[34]. Two important results were published in 1932, the first by Williams[35]. He used specimens made by mixing the powdered elements obtained from the reduced oxides, pressing with sintering, and hot swaging. The final treatment was annealing for two hours in hydrogen at 1000^0 C and cooling slowly. In the second, Masiyama[36] used electrolyte iron and cobalt melted in vacuum with the addition of 0.5% manganese, cast, forged into rods, and machined to ellipsoids. The chief impurities were reported as 'traces'. Annealing was at 1050^0 C in vacuum for 1.5 hours, and cooling was slow. The maximum field strength used in each investigation was around 1300 Oersteds. Williams' curves for magnetostriction, $\frac{\Delta l}{l}$, versus magnetic field,

Figure 4-22. Magnetostriction of various specimens of iron at low and intermediate levels of magnetization.

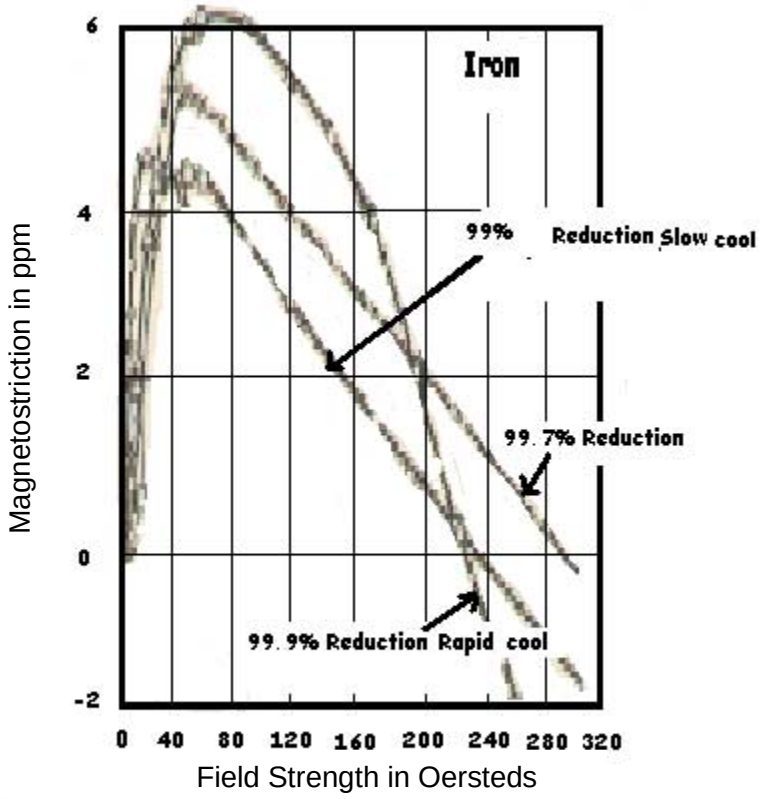

Figure 4-23. This is a portion of the hysteresis loops of magnetostriction in iron. The figure is reprinted from Bozorth (1902).

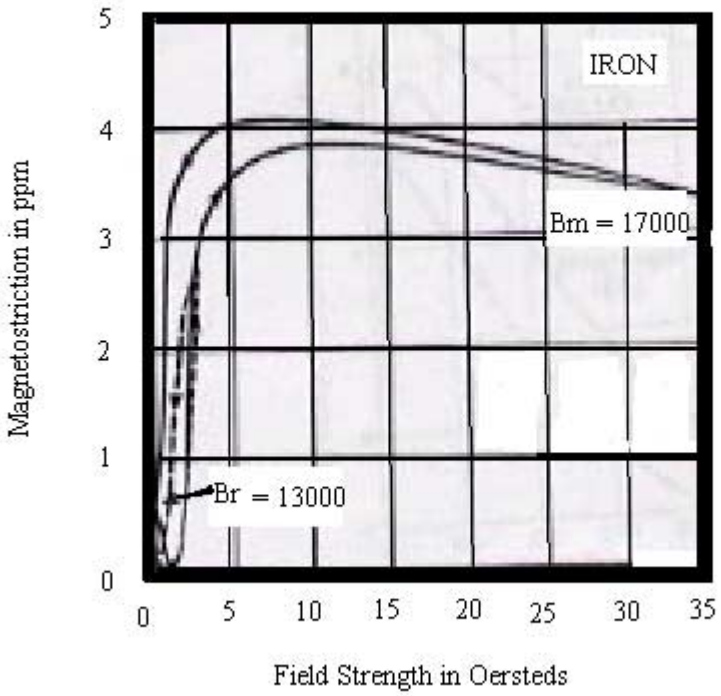

H, for the sake of comparison, are reprinted in Figure 4-24. Masiyama's curves of $\frac{\Delta l}{l}$ versus composition for various field strengths are shown in Figure 4-25. The results show that in high field there is a large magnetostriction of 60-90 ppm due to expansion in alloys containing 40 –70 % cobalt. The highest magnetostriction that has been observed on the order of 130 ppm is in specimens of hard rolled tape containing 70% cobalt. This is because the rolling orients the domains transversely to the direction of rolling, which helps to produce the maximum effect on the magnetostriction.

Iron - Nickel Alloys

Iron and nickel alloys have a special interest on account of the scientific and technical importance of the permalloys, and the related fact that the magnetostriction becomes very small as the nickel content of the alloy approaches 81%. For example, the permalloy which occurs in the magnetostriction graphs of Figures 4-15, 4-16 and 4-17 is an alloy of 46% nickel in iron. Figure 4-26 shows all of the data plotted by Schulze[37] for applied magnetic field strength up to 300 Oersteds. Schulze prepared his specimen (a rod of length 33 cm and of diameter 6 cm) with electrolytic iron and with 99.2% pure nickel, along with the addition of manganese on the order of about 0.4% - 1.7%. It was found that similar results were obtained by Masiyama[38]. The effect of composition on the magnetostriction, where Schulze's data are plotted as dotted lines, was shown earlier in Figure 4-19. This figure shows the characteristic change of sign near 81% nickel and two maxima at near 20% and 45% nickel concentration. It shows that the addition of nickel, which has a negative magnetostriction (contraction), causes an unexpected increase in the

Figure 4-24. The magnetostriction of iron - cobalt alloys plotted against the applied field strength. The figure is reprinted from Bozorth (1932).

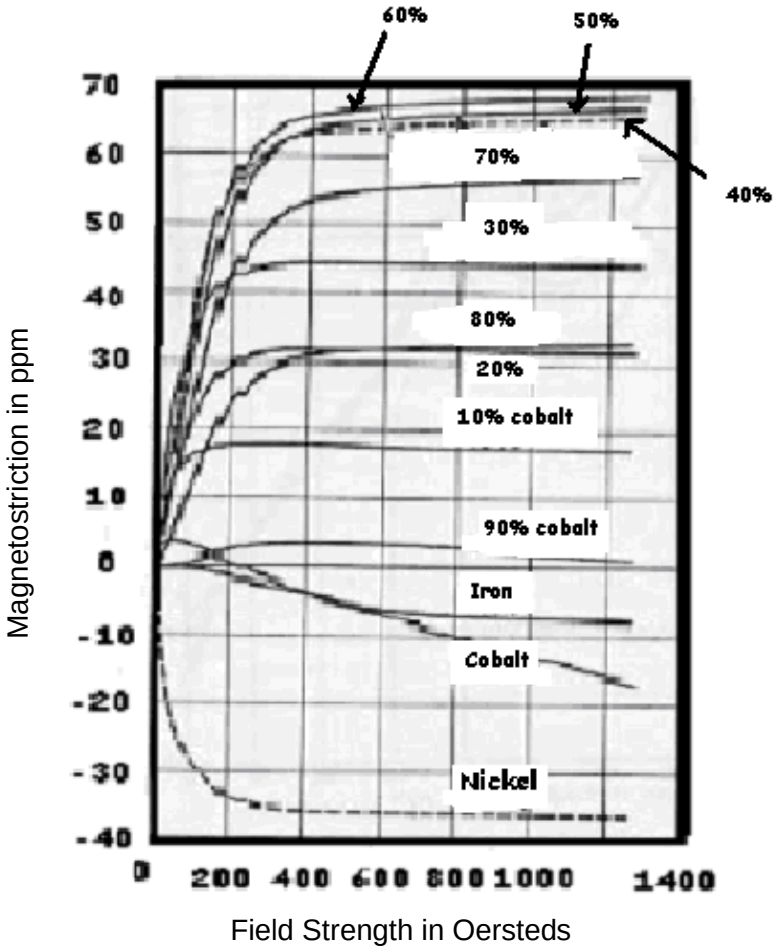

Figure 4-25. The magnetostriction of iron-cobalt alloys vs. the composition according to Masiyama, and the saturation values according to Williams (1930).

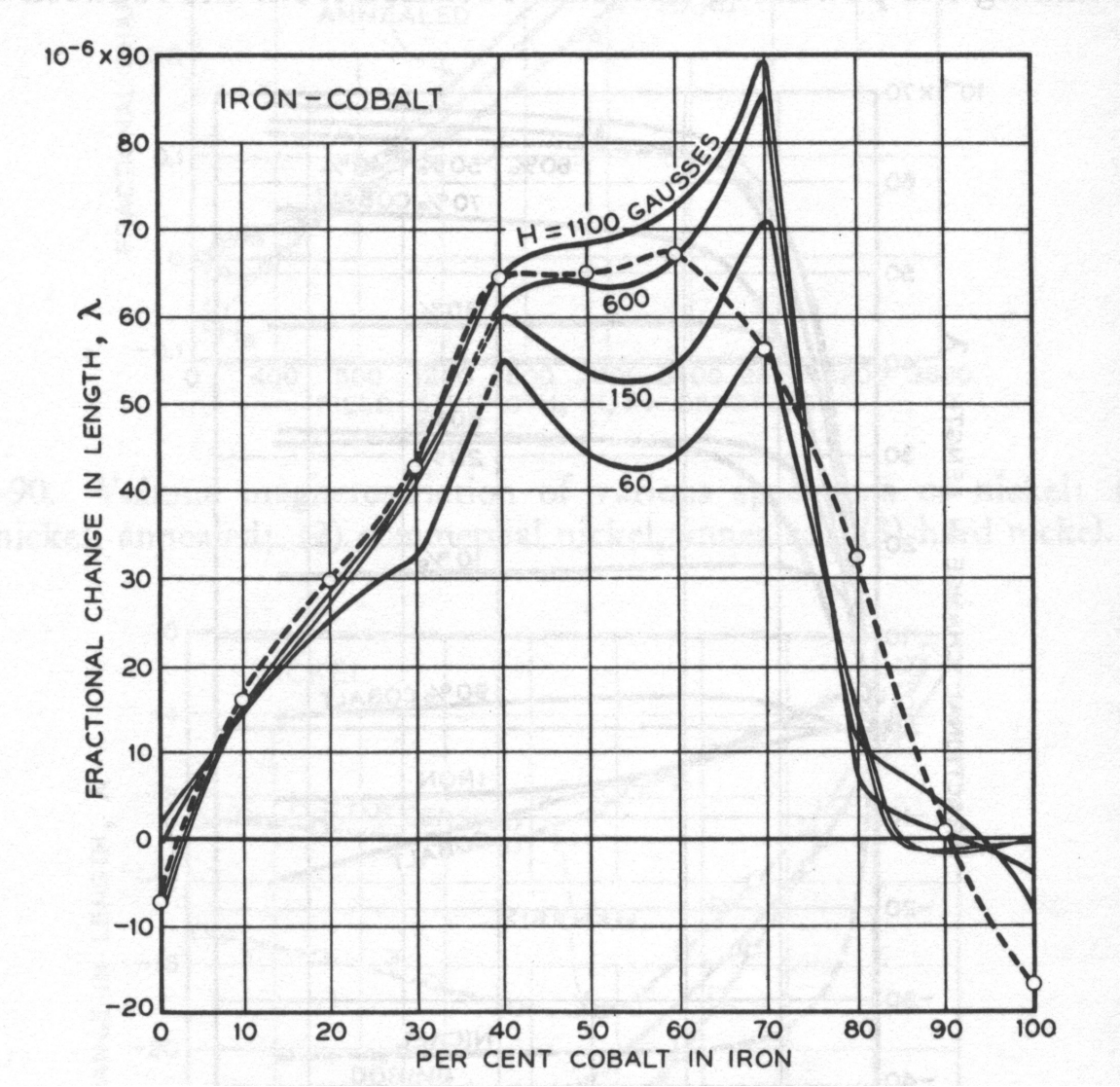

Figure 4-26. The magnetostriction of various iron-nickel alloys. The figure is reprinted from Bozorth (1928).

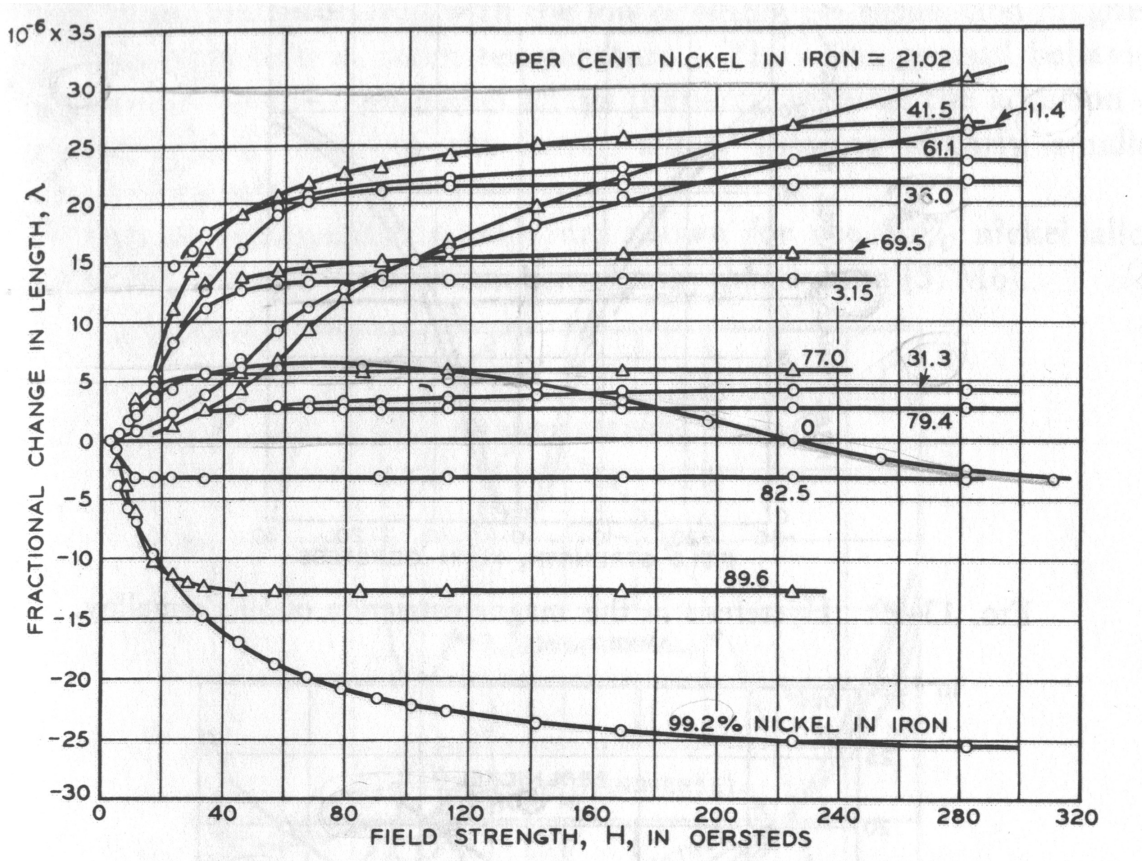

magnetostriction. An addition of only 1-3% of nickel is required in order to eliminate the high field contraction of iron.

These above results show that the magnetostriction level in nickel and cobalt is, in general, larger than that of iron and others. In our case, the results of our experiments match with these earlier results. We observed the level of magnetostriction in pure nickel and the 4340 steel to be 22 ppm and 13 ppm, respectively.

So, from earlier results as well as from our results, it can be concluded that the magnetostriction effect is high in the materials containing high percentages of nickel and cobalt. For the weaker magnetic fields the contraction in nickel has been observed to be less than 30 ppm as shown in Figure 4-15, whereas for higher magnetic fields it has been observed to be around 40 ppm as shown in Figure 4-16. In our case, the magnetic field we generated from the large 60 Hz power supply was reasonably high, so that our magnetostriction measurement of a little over 40 ppm (2×22 ppm $\sim$ 44 ppm) is substantially in agreement with earlier results.

Chapter 5. Conclusion

The phenomenon of magnetostriction was discovered more than 150 years ago, and it was published[39] by J. P. Joule in Philosophical Magazine in 1847. Since that time there has been both the study of the magnetostriction effect in terms of the basic science, and its application in areas such as the generators of sound, magnetoacoustic transforms, actuators for optoelectronic systems, detection and ranging. The recent development of modern technologies, such as microfabrication, and materials, such as rare earth based bulk materials and magnetic thin films, has produced new opportunities for the study and applications of magnetostriction. Similarly, as mentioned earlier it has some practical applications to high frequency oscillators and to generators of supersound, as well as in torque sensors, which can be used in automotive power steering systems and in automotive transmission systems, as mentioned in chapter 1, section 2.

Due to this vast array of applications, measurement of magnetostriction in ferromagnetic materials has become very important these days. Though measurement of magnetostriction is not easy, and can in general be very complex and expensive, in our WIU physics laboratory we have developed a simple and cost-effective method of measuring magnetostriction using a capacitance bridge meter technique as explained earlier in chapter 3, section 4. The results we have obtained using the above techniques were both accurate and in agreement with earlier results. The method we have developed for the fitting and analysis of our experimental data has now been standardized. The magnetostriction values of pure nickel and of a steel alloy containing cobalt and nickel were both large as compared to that of pure iron. In our experiment we used a single ring

for our sample which is the reason for obtaining about 50% of the magnetostriction values supplied in the Bozorth text.

Now that our method of measurement of magnetostriction has been standardized, in the future this method can be used to measure the magnetostriction levels in many different type of steel alloys. This will serve to identify which types of steel alloys will be most applicable for use as torque sensors, and will thus eliminate the usual need for more expensive types of magnetic properties testing for many of these alloys.

References

1. L. W. McKeehan, Phys. Rev. **28**, 158 (1926).
2. Soshin Chikazumi, "Physics of Magnetism", p.173 (1964).
3. S. R. J. Williams, Opt. Soc. Am. **14**, pp. 383-408 (1948).
4. See Ref. 2.
5. K. Honada, Syokwabo and Co., Tokyo, pp. 1-256 (1928).
6. O'Conner and Fawcett, Measure. Sci. Tec. **5** (1994).
7. N. Tsuya, *et al*, Phys. Stat. Sol. (a) **31**, 575 (1975).
8. S. Ishio, et al, J. Mag. & Mag. Mat. **79**, 358 (1998).
9. Frank Jerems, Ph.D. Thesis, University of Hull (1999).
10. M. S. Boley, D. A. Franklin, and D. K. Rigsbee, J. Appl. Phys. **87**, 7073 (2000).
11. R. M. Bozorth, "Ferromagnetism", D. Van. Nostrand Co., Princeton, N.J., (1951).
12. See Ref. 10.
13. Allan H. Morrish, "The Physical Principle of Magnetism", John Wiley and Sons, p.46 (1965).
14. K. J. Sixtus and L. Tonks, Phys. Rev. **42**, 416 (1932).
15. See Ref 14.
16. F. Bloch, Z. Physik. **74**, 295 (1932).
17. See Ref 14.
18. L. Neel, J. Phys. **15**, 227 (1954).
19. S. Chikazumi, "Physics of Magnetism", John Wiley & Sons, p.167 (1964).
20. S. Chikazumi, "Physics of Magnetism", John Wiley & Sons, p.171 (1964).
21. I. J. Garshelis, IEEE Conference on Magnetics (April 2000).

22. M. V. Klein, "Optics", John Wiley & Sons, p. 495 (1970).

23. Won-Chul Shin, "Magnetostriction effects in high speed steels and nickel doping in YBCO superconductors", M. S. Thesis, WIU Physics Department, p. 29 (2001).

24. See Ref. 23.

25. R. M. Bozorth, "Ferromagnetism", (D. Van Nostrand Company, Inc.), Princeton, New Jersey, p. 632 (1968).

26. See Ref. 25.

27. See Ref. 25.

28. See Ref. 25.

29. H. Masumoto and S. Nara, Sci. Repts. (Tohoku Imp.Univ.) **16**, 333 (1931).

30. Y. Masiyama, Sci. Repts. (Tohoku Imp. Univ.) **26**, 1 (1937).

31. R. M. Bozorth, "Ferromagnetism", (D. Van Nostrand Company, Inc.), Princeton, New Jersey, p. 660 (1968).

32. W. Fricke, Z. Physik **80**, 324 (1933).

33. K. Honda, K. Kido, Sci. Repts. (Tohoku Imp. Univ.) **9**, 221 (1920).

34. A. Z. Schulze, Tech. Physik **8**, 495 (1927).

35. S. R. Williams, Rev. Sci. Instruments **3**, 675 (1932).

36. Y. Masiyama, Sci. Repts. (Tohoku Imp. Univ**.**) **21**, 394 (1932).

37. A. Schulze, Z. Physik **86**, 798 (1928).

38. Y. Masiyama, Sci. Rept. (Tohoku Imp.Univ.) **20**, 574 (1931).

39. J. P. Joule, Phil. Mag. **30**, 76 (1847).